9 Strain Rates from GPS

This Section presents our use of GPS data to quantify the rates of tectonic deformation in Kyushu. We overview the GPS data used, review the elastic block model approach to interpret the data and remove elastic strain effects from subduction coupling. We have developed a logic tree for estimation of rock deformation strain in Kyushu from GPS, involving 120 different GPS strain models. For each of these strain models, we have estimated and removed the influence of elastic strain due to subduction zone coupling from the GPS velocity field using a variety of elastic block model configurations, which we also outline here. We show a weighted average of the logic tree results, in terms of areal strain, shear strain, and the 2nd invariant of the strain tensor. We also show the distribution of strain values at several example locations in the region, and discuss these results within the context of the tectonic setting of the region. We also present a hypothesis for the existence of a high shear strain zone in southern Kyushu detected by GPS.

9.1 GPS Data Used

Velocities of GPS sites throughout Japan are derived from combination of SINEX (Solution INdependent EXchange format) files provided to us by the Geographical Survey Institute (GSI; http://mekira.gsi.go.jp/) from their daily processing of the Geonet Continuous GPS (CGPS) network in Japan (~1200 CGPS sites in total). The daily network processing of the Geonet network is conducted by GSI, with Bernese GPS processing software (Rothacher and Mervart, 1996; Beutler et al., 2001) using standard processing methods. The SINEX files we use are from one day every three months for the period 1996-2004. In order to combine the daily SINEX files to estimate velocities for the CGPS sites in Japan relative to a known terrestrial reference frame, we use GLOBK software (e.g., Herring, 2001).

To help place the Japanese dataset in a global context, we also use daily solutions from Scripps Institute of Oceanography processing of the global IGS network of GPS sites (http://sopac.ucsd.edu), as well as SINEX files from processing of a subset of ~10 Japanese sites and several global sites that have been submitted by GSI to the Crustal Dynamics Data Information System (CDDIS; http://cddis.gsfc.nasa.gov/). Using GLOBK we estimate a rotation and translation of each dataset into the ITRF2000 reference frame (Altamimi et al., 2002), for each day. To accomplish this, we tightly constrain the coordinates of a subset of the most reliable IGS GPS stations to their known ITRF2000 values. We do this for each set of daily solutions, obtaining a time series of site positions in the ITRF2000 reference frame. The ITRF2000 velocities at each GPS station are calculated by a linear fit to the daily ITRF2000 coordinates. The uncertainties in the linear fits are derived using a white-noise model, so the uncertainties are seriously underestimated (e.g., Zhang et al., 1997; Williams et al., 2004). We multiply the formal uncertainties by 5 to give “reasonable” values of about 1 mm/a uncertainty in horizontal velocities for long-running stations within Japan (T. Nishimura, pers. comm., 2005). Ideally, the GPS velocity errors should be assessed more rigorously. This will require maximum-likelihood analysis of (probably daily, perhaps weekly) time series of GPS positions, to define the appropriate noise model for the data and to calculate a realistic velocity uncertainty (e.g., Williams et al., 2004; Langbein, 2004).

It is important to avoid the effects on our velocity estimates from large earthquakes and slow slip events. The major events influencing the GPS time series in Kyushu from 1996-2003 are two large thrust earthquakes (M_s 6.7) near Hyuga-nada in 1996 (e.g., Yagi et al., 2001), the 1996-1997 Bungo Channel slow slip event (e.g., Hirose et al., 1999), and the 1997 Kagoshima-ken-hokuseibu earthquake (Fujiwara et al., 1998). To remove the influence of coseismic displacements from the time series, we removed the time series data prior to 1998 in the regions affected by these events. GPS sites in the Kagoshima region were affected by an inflation event at Aira caldera throughout the GPS measurement period (Kriswati and Iguchi, 2003); we used Mogi source parameters for the inflation event estimated by Nishimura et al. (2004) to remove this effect from the dataset. We also conducted a visual inspection of the daily position time series for all the sites in the Kyushu and southwest Honshu region to be sure that there was no non-linear behaviour recorded by the GPS sites that is not representative of steady movement during the interseismic period.

To interpret the GPS site velocities in a tectonically meaningful way, it is important to place the velocities into a “plate-fixed” reference frame (in this case, we choose Eurasia-fixed). We do this at the inversion/tectonic modelling stage of this work (see Section 4) by estimating a rotation of the entire dataset that minimizes the velocities at sites known to be on the stable Eurasian Plate. The GPS velocity field in southwest Japan is shown in a Eurasia-fixed reference frame in Figure 9.1.

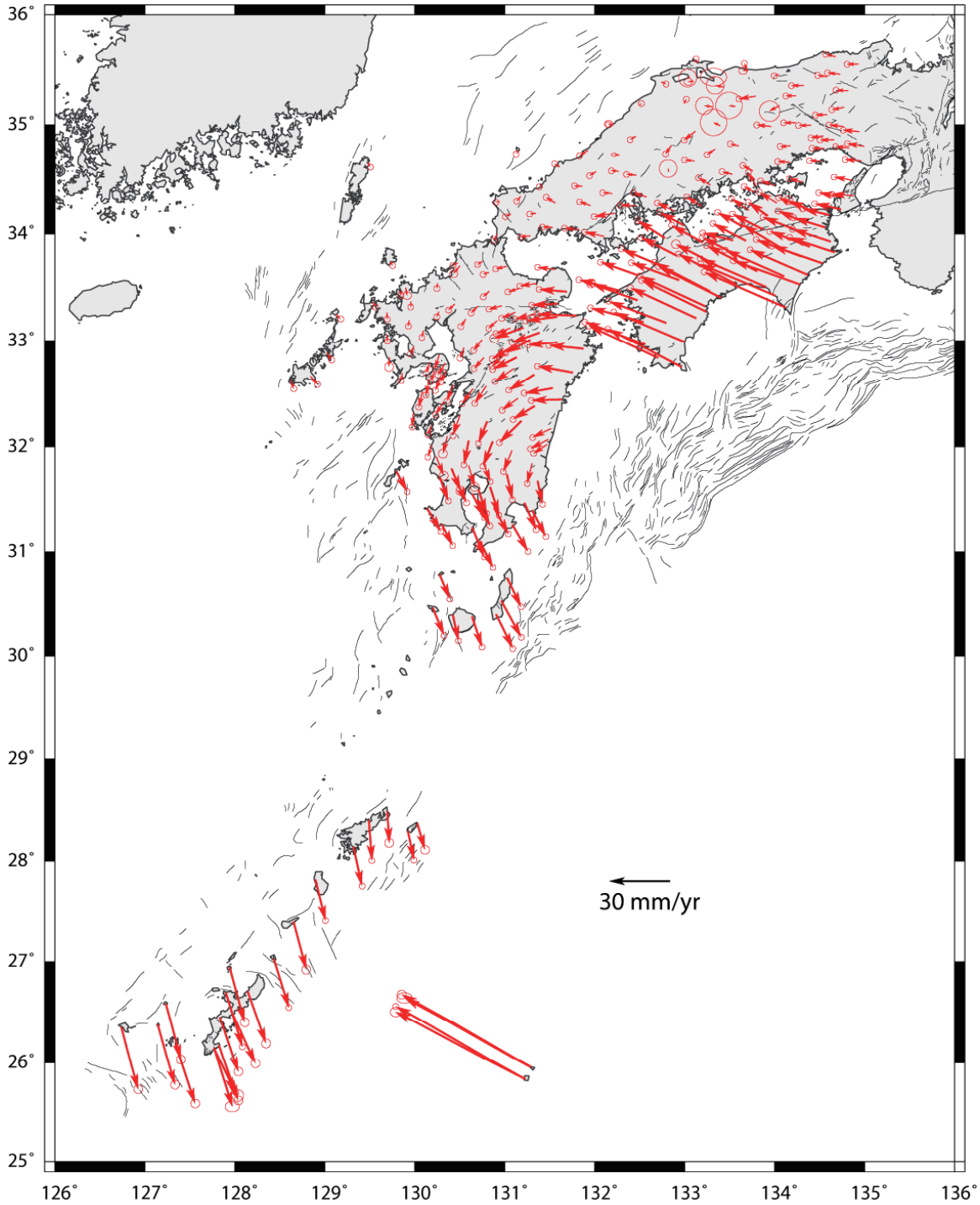

Figure 9.1: The GPS velocity field for southwest Japan (relative to the Eurasian Plate). Thin black lines show active faults.

In addition to the GPS velocities described earlier, we use published GPS velocities in the inversion from Heki et al. (1999), Calais et al. (2003), Sella et al. (2002), Beavan et al. (2002), and Prawirodirdjo et al. (2004). These datasets help us to further place the southwest Japan GPS dataset into a regional plate kinematic context. This is critical as we must be sure to account for all of the possible relative motion between the various tectonic plates in the system that could be influencing the GPS measurements in Japan.

In addition to the GPS velocities we also include earthquake slip vectors from events on the Nankai Trough and Ryukyu Trench (from Harvard CMT, http://www.globalcmt.org/CMTsearch.html) as these data give us information about the relative motion between the Kyushu forearc relative to the underthrusting Philippine Sea Plate. We also include slip vector data for the Median Tectonic Line (MTL) in Shikoku that is consistent with the geological observations of nearly pure right-lateral slip on that fault.

9.2 Approach Used to Model GPS Data in Kyushu

Large, complex strain patterns are apparent in the GPS strain map in southwest Japan (Figure 9.2). However, much of this strain is related to interseismic coupling on the offshore subduction zone boundary. To isolate the strains that may reflect permanent deformation of the upper plate, we must remove this effect.

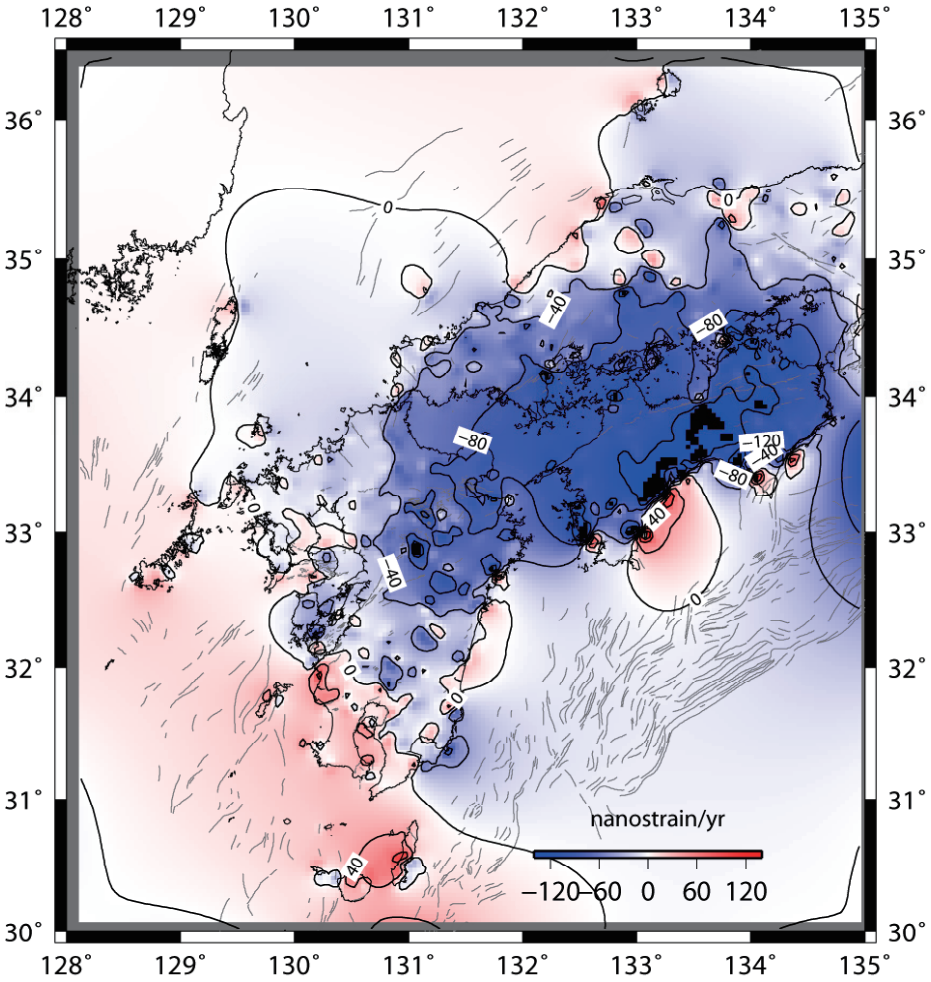

Figure 9.2(a): Areal strain rates (in nanostrains/a) from the raw GPS velocity field (Figure 9.1; no elastic strains removed) estimated using the Haines and Holt method.

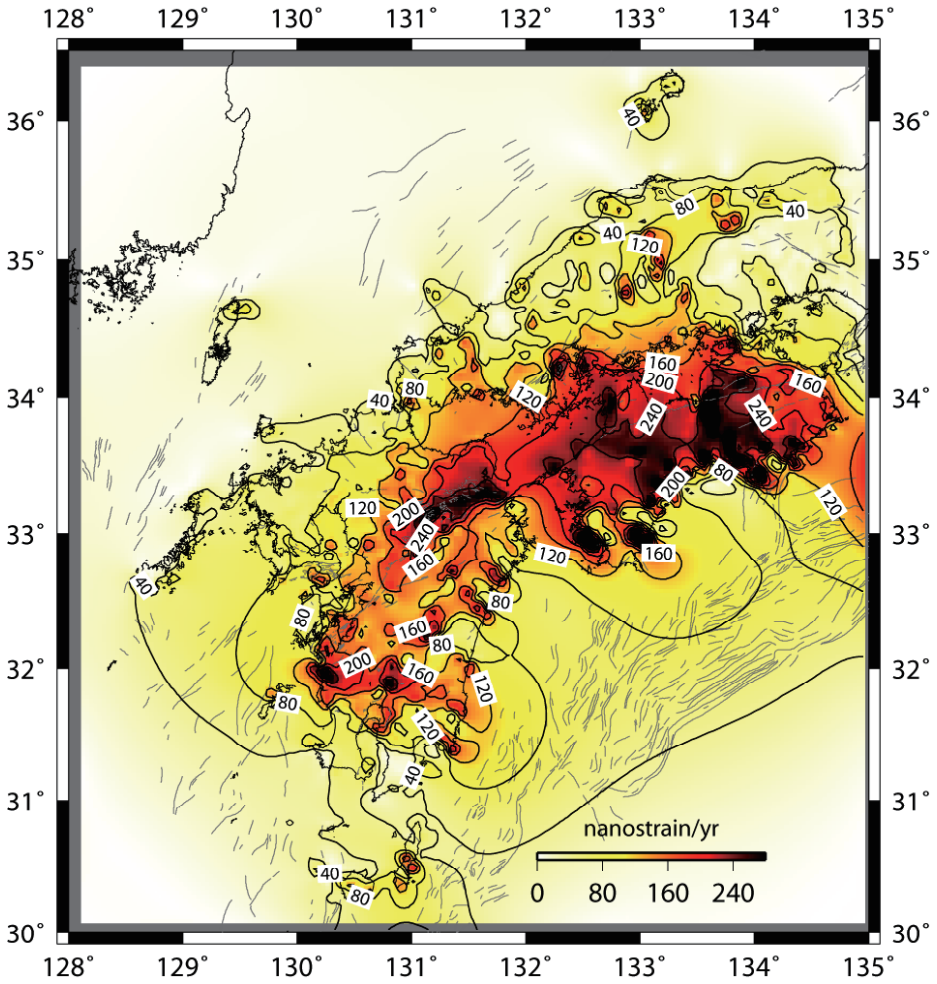

Figure 9.2(b): Shear strain rates (in nanostrains/a) from the raw GPS velocity field (Figure 9.1; no elastic strains removed) estimated using the Haines and Holt method.

Recently, many studies have shown that GPS velocities measured in zones of active faulting during the interseismic period are explained by interseismic elastic strains, as well as long-term rotation of crustal blocks in the deforming zone (e.g., McCaffrey et al., 2000; McCaffrey, 2002, 2005; McClusky et al., 2001; Meade and Hager, 2005; Wallace et al., 2004, 2007). Methods have been devised by McCaffrey (1995, 2002) and Meade and Hager (2005) to invert GPS velocities for long-term rotations of tectonic blocks, and elastic strain due to coupling on block-bounding faults. Recently, Nishimura and Hashimoto (2006) have used a similar method to the elastic block approach for interpreting GPS velocities in Kyushu. For the purposes of rock deformation/tectonic hazards assessment, if the elastic deformation estimated from the inversion for the fault coupling parameters is subtracted from the original GPS velocities, the resulting velocity field will be approximately free of the elastic effects of interseismic coupling on known, major active faults in the region. These residual velocity and strain-rate fields may be interpreted in terms of deformation due to other minor faults or perhaps zones of distributed deformation.

McCaffrey's (1995, 2002) method performs a non-linear inversion to simultaneously estimate the angular velocities of elastic blocks and coupling coefficients on block-bounding faults, to give the best fit to the GPS velocities, and optionally, earthquake slip vectors, and geological fault slip rates and azimuths. The data misfit, defined by the reduced chi-squared statistic (χ_n^2), is minimised. The method also allows us to optimally rotate multiple GPS velocity solutions into a common reference frame. McCaffrey's approach also has the benefit of including all of the bounding plates so that we can establish the plate motion budget that needs to be accounted for in the plate boundary zone. Once the elastic deformation effects due to interseismic coupling on the Ryukyu Trench and Nankai Trough (estimated using the elastic block method) have been removed from the GPS velocity field, the residual strain (largely due

to possible upper-plate deformation) can be mapped using a variety of methods (e.g., Haines and Holt, 1993; Beavan and Haines, 2001; Sagiya et al., 2000; Miura et al., 2004). Given the uncertainties inherent in GPS measurements, GPS techniques are unable to reliably detect strain rates below a certain threshold (this threshold will be dependent on the quality of the GPS network and data and distribution of GPS sites); thus, GPS should not be used on its own to determine if a site is tectonically stable (i.e., additional geological and seismological investigations will be needed to confirm tectonic stability.)

9.3 Elastic Block Model Set-up for Kyushu

We have investigated six different elastic block model configurations for the southwest Japan region. In all of the models, we define a Eurasian Plate, Amurian Plate, Philippine Sea Plate, Southwest Japan Block, and Okinawa Block (Figure 9.3).

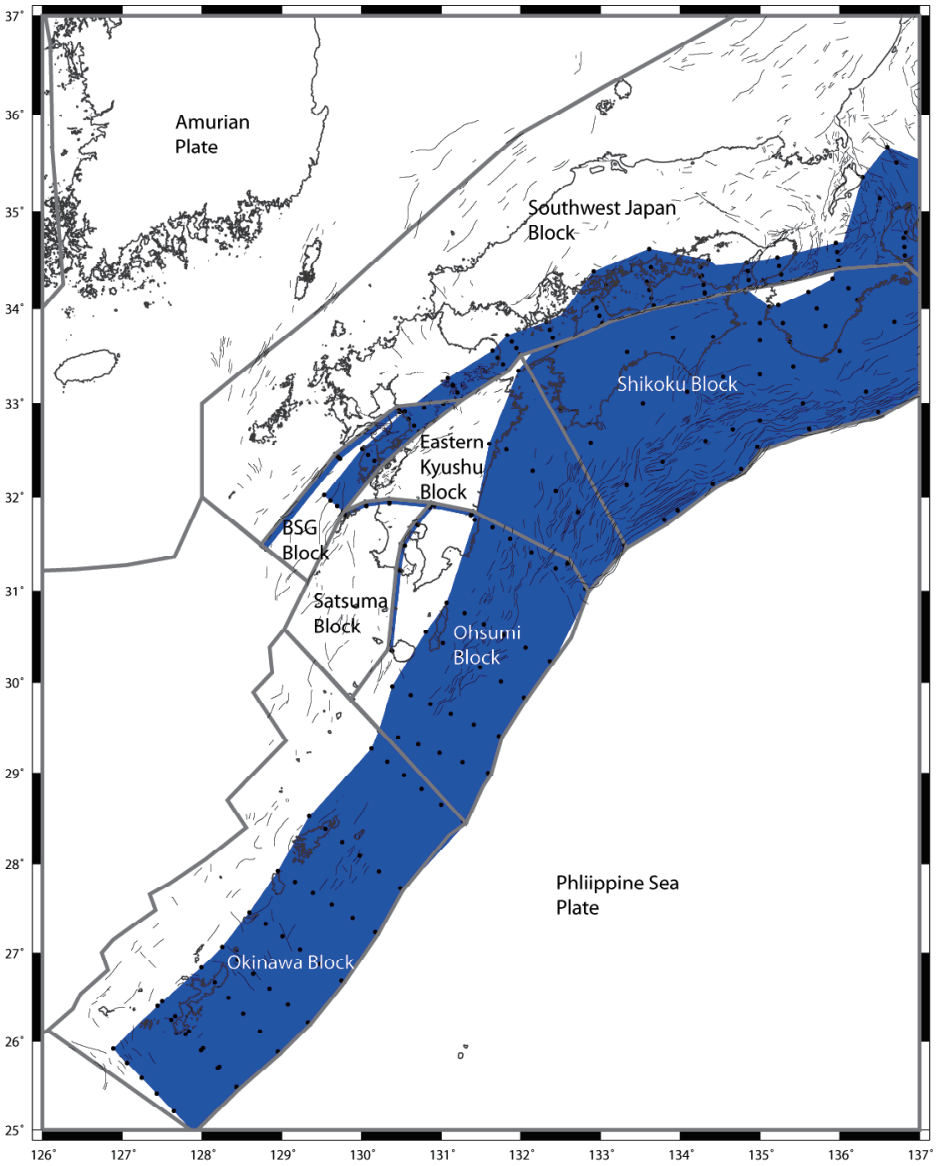

Figure 9.3: Block model set-up for southwest Japan, where the southwest Japan forearc is divided into four separate blocks. Note, we have conducted six different models where various combinations of these blocks are connected together, forming composite blocks (see discussion in text). Dark grey lines are block boundaries, blue planes are a plan-view of faults used in the model (black dots represent nodes defining the fault planes).

We define most of the boundaries of the large plates (Amurian, Philippine Sea and Eurasian Plates) based on a digital compilation of tectonic plate boundaries by Bird (2003). The

inclusion of these larger plates also helps us in establishing the overall plate motion budget that must occur across the plate boundary zone in southwest Japan. The Southwest Japan/Amurian Block boundary is defined by a zone of distributed faulting near the west coast of Japan (Gutscher and Lallemand, 1999), which is also associated with strike-slip events (probably right-lateral, striking parallel to the margin; Figure 9.4).

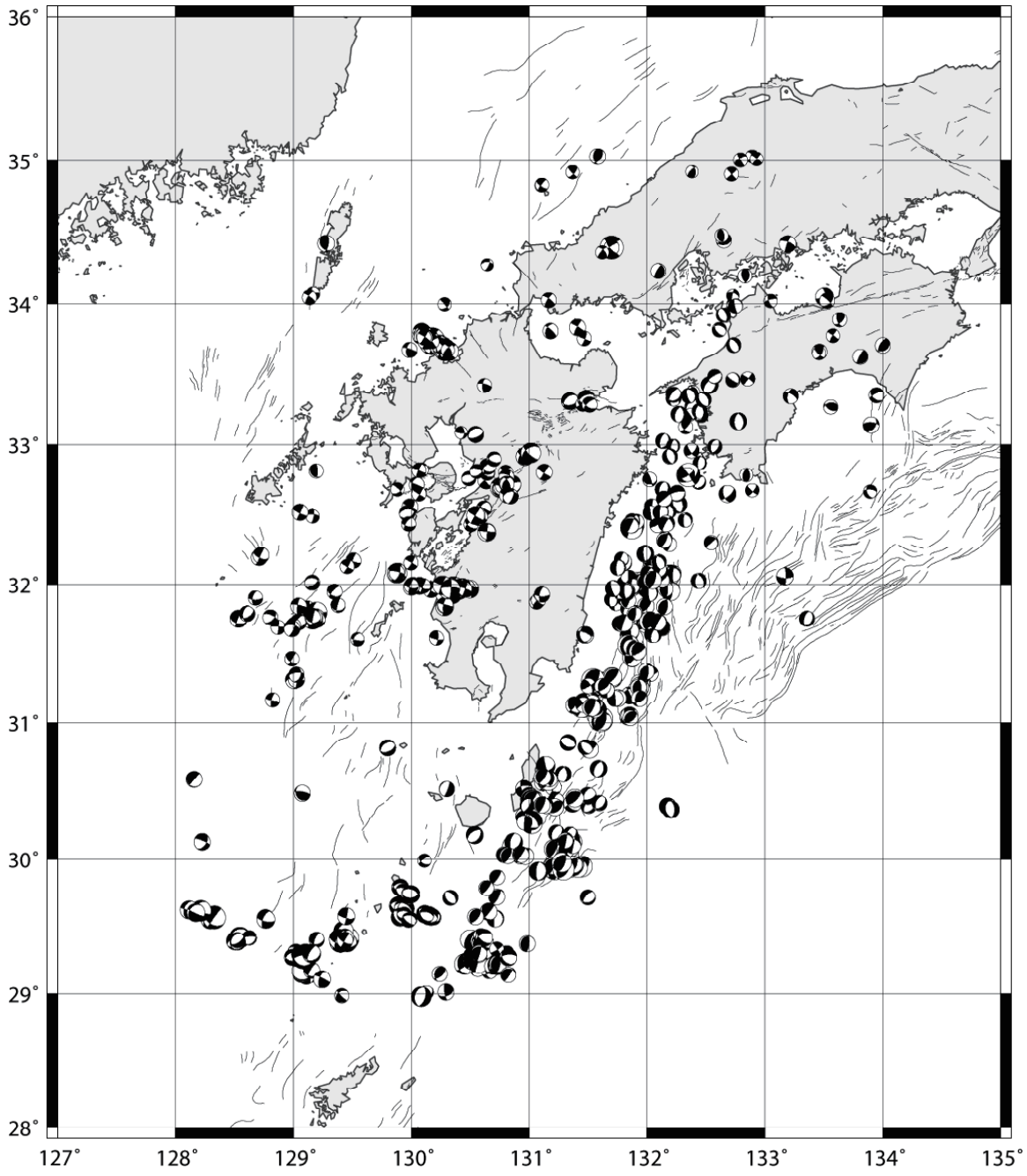

Figure 9.4: Focal mechanism plots for earthquakes in southwest Japan from 1997-2006. Based on CMT solutions from the JMA catalogue (data from http://www.fnet.bosai.go.jp).

The distinction between the models we have conducted here is based upon the division of the forearc and backarc blocks in southwest Japan. For the most complex model, we have

broken the southwest Japan forearc and backarc region into four different blocks (Figure 9.3; Table 9.1), including the Shikoku block, eastern Kyushu block, Ohsumi, and Satsuma blocks, and have divided the backarc into two blocks (the Beppu-Shimabara Block and the Southwest Japan block).

The Shikoku block is bounded to the northwest by the MTL. The Ohsumi block is bounded on the west by the Kagoshima Graben, and on the north by a possibly active left-lateral shear zone that has been highlighted by earthquakes and GPS measurements (e.g., Kodama et al., 1995; Nishimura and Hashimoto, 2006).

We use the Kagoshima graben as a boundary in some of our models based on evidence from GPS (Figures 9.1 and 9.2) and geology (Aramaki, 1984) for active extension in the Kagoshima Graben, and paleomagnetic evidence that southeast Kyushu has rotated independently of the rest of Kyushu for the last 2-6 Ma (Kodama et al., 1995). The Satsuma block is bounded on the east by the Kagoshima graben and on the north by the hypothesised active left-lateral shear zone. The eastern Kyushu block encompasses more than half of the Kyushu forearc, whose western boundary is the southeastern boundary of the Beppu-Shimabara graben.

We have conducted ten different block model scenarios, testing various block combinations (Table 9.1). For example, Model 1 considers the Satsuma, Ohsumi, eastern Kyushu and Shikoku blocks as one composite block. Table 9.1 summarizes the fits to the GPS and earthquake slip vector data in terms of the reduced chi-squared statistic (χ_n^2). In Section 9.4, we discuss the results of the best-fitting block model in further detail.

To define the subduction interface fault (Nankai and Ryukyu Troughs), we approximate the configurations for the Nankai subduction interface in Sagiya and Thatcher (1999) and Shiomi et al. (2004) (Figure 9.3). On the subduction interface, we specify individual nodes defining the interface spaced on average 50 km apart along strike, and at 10 km depth intervals between 0 and 50 km depth (Figure 9.3). We define the MTL as a northward dipping fault, based on geophysical evidence (Ito et al., 1996; Onishi et al., 1999; Tabei et al., 2002).

For the purposes of this initial study, we approximate the boundaries of the Beppu-Shimabara Graben (BSG) block as a single fault on each boundary in the model, although more complex deformation on several faults across a zone is likely to be a more realistic scenario there. We set the southern BSG fault to dip northwest, in part, to deal with possible distributed deformation due to faulting within the BSG block itself.

McCaffrey's (2002) method is used to solve for coupling coefficients at nodes on the Nankai and Ryukyu troughs, the faults representing the BSG boundaries, the extensional zone in the Kagoshima Graben, the MTL, and a possible zone of left-lateral strike-slip cross-cutting southeast Kyushu (Figure 9.3). To represent the change in coupling coefficient (ϕ) values between adjacent nodes, ϕ values on 5 km x 5 km rectangular fault patches between the nodes are estimated by bilinear interpolation.

Additional free parameters in the inversion are the rotation parameters (three for each block) for various combinations of the Amurian Plate, Southwest Japan Block, Shikoku block, Pacific Plate, eastern Kyushu, Beppu-Shimabara Graben, Ohsumi and Satsuma blocks relative to Eurasia, and rotation parameters that rotate each GPS velocity dataset into a Eurasia-fixed reference frame.

Table 9.1: Description and fits to the data of the six different block configurations tested. SATS = Satsuma block; OHSU = Ohsumi block; SHIK = Shikoku block; KYUS = Eastern Kyushu block; SWJP = Southwest Japan block; BSG = Beppu-Shimabara Graben block. The block configurations are explained in terms of whether adjacent blocks are connected as a single, composite block, or whether they represent an independent block. For example, if the line in the table says "SATS+OHSU", it means that the Satsuma and Ohsumi blocks are combined into a single block, while if the line says "SATS" the Satsuma block is independent of the other blocks. χ_n^2 is the reduced-chi squared for each best-fitting model using the prescribed block configuration.

Model Number	Block configuration	χ_n^2	Number of independent blocks in SW Japan
1	SATS+OHSU+KYUS+SHIK BSG+SWJP	5.49	2
2	SATS+OHSU KYUS+SHIK BSG+SWJP	2.07	3
3	SATS+OHSU KYUS+SHIK BSG SWJP	3.13	4
4	KYUS+SHIK SATS OHSU BSG+SWJP	2.17	4
5	KYUS+SHIK SATS OHSU BSG SWJP	2.31	5
6	SATS+OHSU+KYUS BSG+SWJP SHIK	2.4	3
7	SATS+OHSU BSG+SWJP KYUS SHIK	1.9	4
8	SATS+OHSU BSG SWJP KYUS SHIK	2.5	5
9	KYUS SHIK SATS OHSU BSG+SWJP	1.7	5
10	KYUS SHIK SATS OHSU BSG SWJP	1.95	6

9.4 Block Modelling Results for the Best-Fitting Tectonic Model

In general, the models with increasing complexity (i.e., more blocks) appear to produce an improved fit to the data (Table 9.1). This is not unexpected given that there is an increase in the number of free parameters with increasing block model complexity. The best-fitting model (Model 9) is where all four of the forearc blocks (Shikoku, eastern Kyushu, Ohsumi and Satsuma) are independent of one another. The worst-fitting model occurs where all of the forearc blocks constitute a single tectonic block (including Shikoku; Model 1). Models 2 and 7 are similar to the block configuration considered by Nishimura and Hashimoto (2006).

When we break the Kyushu forearc into four separate blocks (Model 9), the fit to the GPS velocities is much better (χ_n^2 = 1.7) than any of the other block model configurations (Table 9.1). In this (the preferred model) 92 free parameters are estimated from 1251 data. The interseismic coupling distribution that we estimate for the Nankai Trough subduction interface (Figure 9.5) is similar to that obtained from previous studies (Nishimura and Hashimoto, 2006).

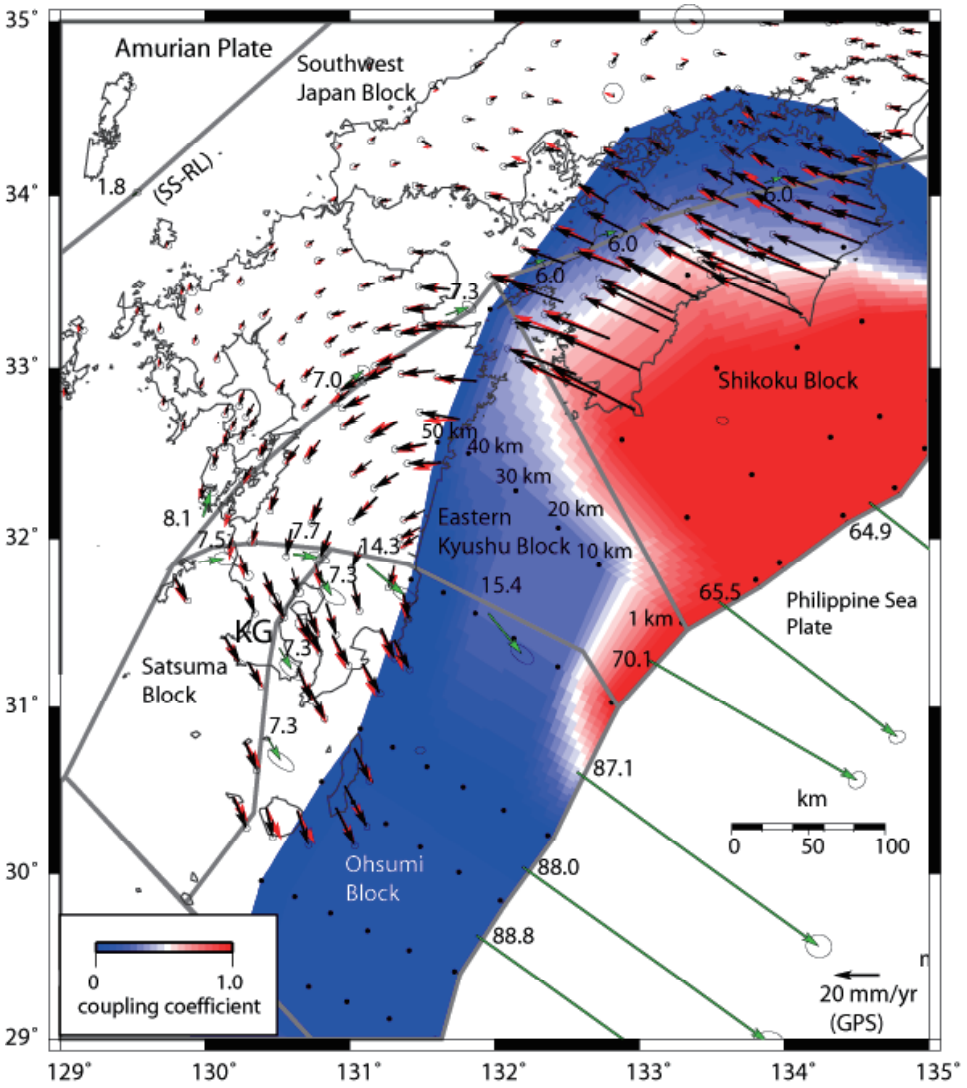

Figure 9.5: Interseismic coupling distribution (in terms of slip rate deficit, mm/a) for the subduction zone from the best-fitting block model (model 9, Table 9.1). Also shown are observed GPS velocities (black), velocities from best-fitting model (red), and relative motion at block boundaries (green, labelled arrows in mm/a). Depth labels for one set of nodes on the subduction zone are shown. Note that the scale for the GPS (observed and modelled) is not the same shown as for the relative block motion vectors. SS-RL = Strike slip-right lateral; KG = Kagoshima Graben.

The interseismic coupling on the subduction interface exerts a great influence on the GPS velocity field (Figure 9.6). The convergence rates we estimate for the Nankai and Ryukyu Troughs are ~70-89 mm/a (Figure 9.5). The rate we estimate for the MTL is ~6 mm/a of pure right-lateral strike-slip, which is in excellent agreement with geological estimates of 5-10 mm/a (Okada, 1970; 1973). This model requires ~7-8 mm/a of right-lateral strike-slip in the eastern BSG, which gradually transitions to more northerly directed extension at up to 8 mm/a. North-south directed extension in the BSG is consistent with focal mechanisms of normal faulting events there (Figure 9.4).

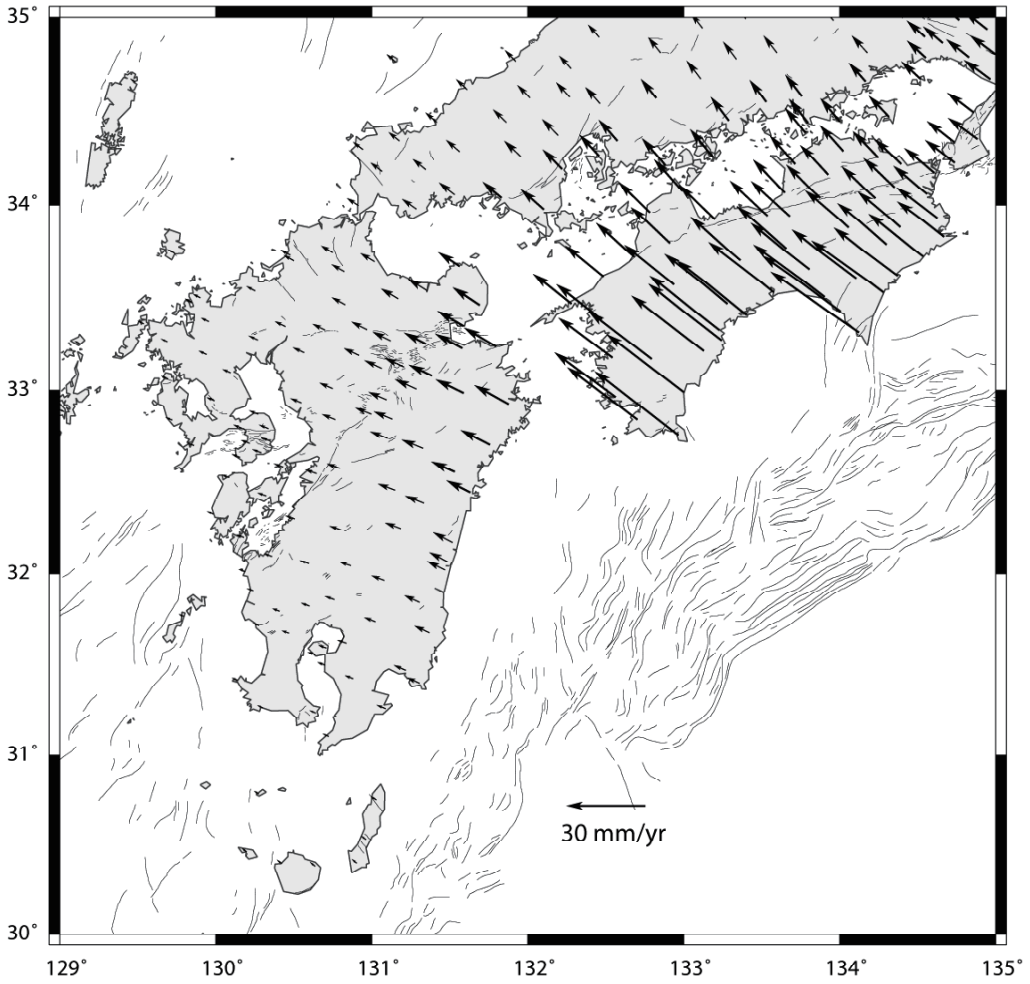

Figure 9.6: Influence on GPS velocities from interseismic coupling distribution in Figure 9.8 shown for the best-fitting model (Model 9, Table 9.1).

The Kagoshima Graben accommodates ~7 mm/a of slightly oblique extension in the best-fitting block model. On the northern boundary of the Ohsumi and Satsuma blocks, ~7-14 mm/a of left-lateral strike-slip is required. The superior fit to the GPS data in Models 2, 4, 5, 7, 9 and 10 compared with Models 1 and 6 (Table 9.1) suggests that left-lateral shear on the northern boundary of the Ohsumi and Satsuma blocks is required by the GPS data (i.e., that the southern Kyushu forearc is a tectonic block independent from the northern Kyushu forearc). The data are well-fitted by ~2 mm/a of right-lateral strike-slip on the offshore Amurian Plate/Southwest Japan block boundary. Due to the small dimensions of the Satsuma and Ohsumi blocks, it is difficult to determine uniquely (with GPS) if the anti-clockwise rotation of southern Kyushu documented in paleomagnetic studies is ongoing today. For example, we are able to fit the GPS data in the Ohsumi block equally well with rapid (~5°/Ma) anti-clockwise vertical axis rotation, and with minimal vertical axis rotation (<0.2°/Ma). However, our best-fitting models do require ~2° per Ma of anticlockwise rotation of the Eastern Kyushu

block about a nearby pole relative to the large, bounding plates (e.g., at 133.86 E, 31.85 S relative to Eurasia).

9.5 Upper Plate Strains in Kyushu

To estimate the strain field due to possible tectonic deformation in Kyushu, we remove the component of the velocity field due to interseismic coupling on the offshore subduction boundary (Figs. 9.5 and 9.6) using Model 9 as an example (Figure 9.7).

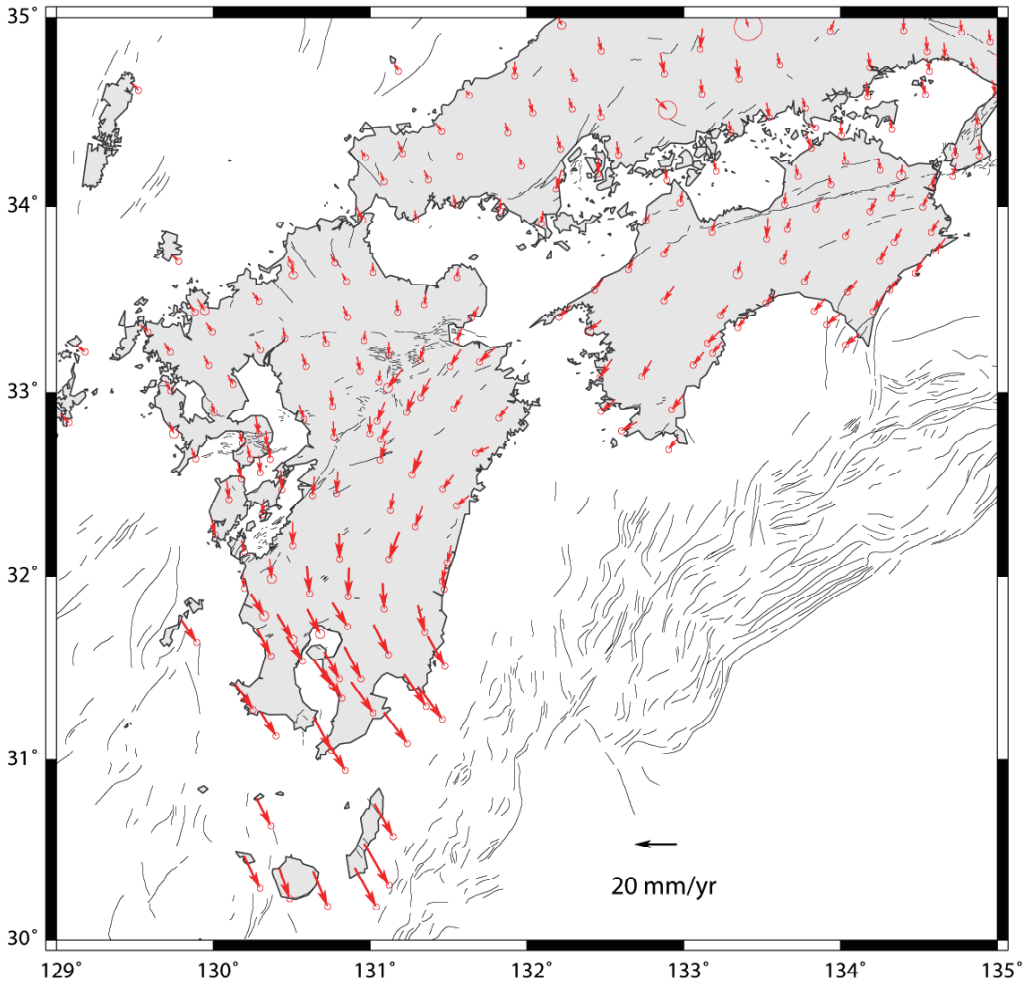

Figure 9.7: GPS velocity field after the component due to interseismic coupling on the subduction zone has been removed (Figure 9.6). This is the velocity field that goes into the Haines/Holt strain modelling (Figures 9.8 and 9.9). Shown for model 9 only.

There are a variety of methods that can be used to convert GPS site velocities to a map of regional strain. Perhaps the most widely used method is one developed by John Haines and Bill Holt (e.g., Haines and Holt, 1993; Beavan and Haines, 2001). To employ their method, a grid (in latitude-longitude) is developed over the area of interest; for the purposes of the Kyushu Case Study, we use a ~5 km x ~5 km grid. Velocities are modelled as bi-cubic splines within each cell, and the inversion attempts both to match the input velocity data and minimize the strain rates within each cell. A strain-rate variance parameter ($1/\nu$ in the terminology of Beavan and Haines, 2001) is defined, with lower values of $1/\nu$ giving smoother solutions. The strain-rate variance parameter is chosen such that the sum of squared residuals between the model and input GPS velocities plus the sum of squares in matching the strain-rate constraints is approximately equal to the number of degrees of freedom in the GPS data set

(i.e., twice the number of velocities). In other words the reduced chi-squared statistic, χ^2_N = (sum of squared residuals)/(degrees of freedom), is approximately equal to 1.

Figure 9.2 shows the shear and areal strain rates for the GPS velocity field without removing the elastic strain due to offshore fault coupling. Clearly, these strain rates are quite high (> 200 nstrain/a), but as discussed previously in this report, much of the strain is related to elastic strains from interseismic coupling on the major offshore subduction faults (Nankai and Ryukyu Troughs) and are unlikely to lead to permanent deformation in the same location where the strain is currently accumulating.

Figures 9.8 and 9.9 show the strain field (areal and maximum shear strain components) after the elastic part of the GPS velocity field due to interseismic coupling (using Model 9) has been removed from the raw velocity field.

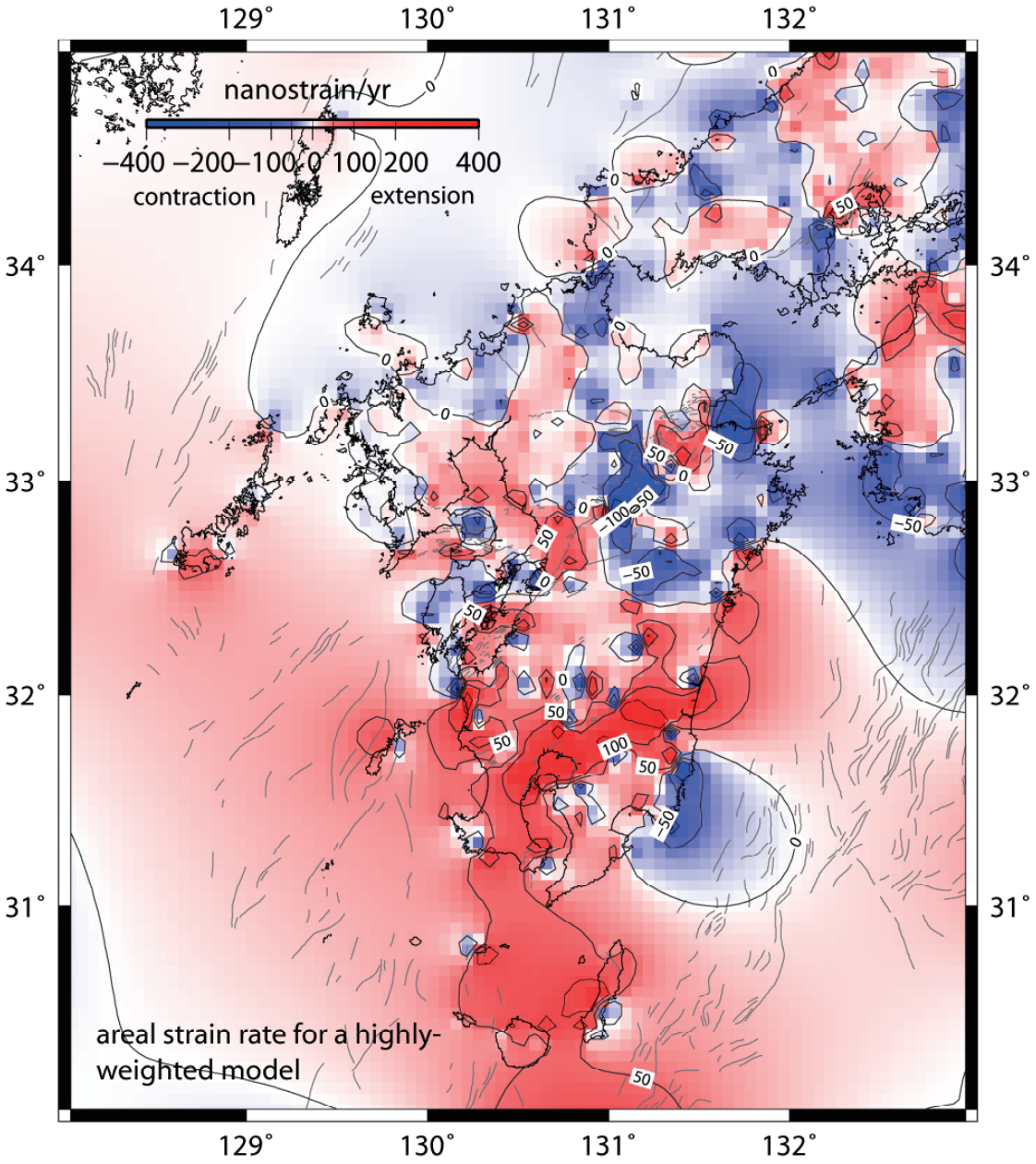

Figure 9.8: Areal strain calculated from the velocity field in Figure 9.7 (with subduction-related elastic strains removed).

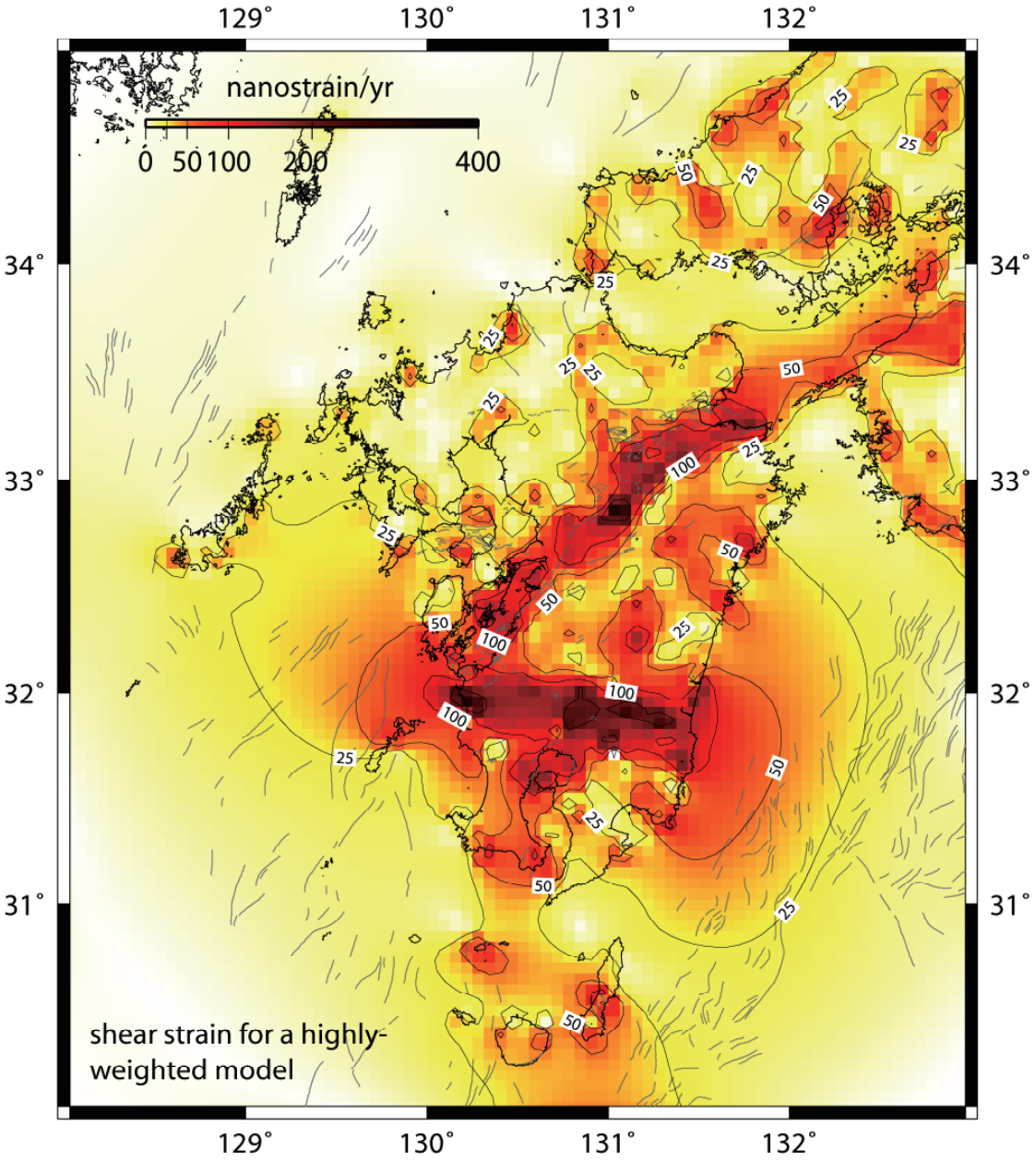

Figure 9.9: Maximum shear strain calculated from the velocity field in Figure 9.7 (with subduction-related elastic strains removed).

The shear strain rate is greatly reduced (Figure 9.9), although the high shear strain zone cutting across southern Kyushu (near the northern boundary of the Ohsumi and Satsuma blocks) is still present, as is a band of elevated shear strain in the region of the MTL and the BSG, consistent with observed strike-slip faulting there. The areal strain maps show high (up to ~50 nanostrains) extensional strain in the Kagoshima Graben region, and a broad zone of residual extensional strain in the western half of the Beppu-Shimabara Graben.

9.6 Tectonic implications

One of the notable results of this study is the discrepancy between the strain rates and fault slip rates estimated from the GPS velocities (Figures 9.5, 9.8 and 9.9) compared with the geological slip rates from the Active Fault Research Centre (AFRC) database (Figure 9.10). Geological studies indicate ~1-3 mm/a of extension and strike-slip in the Beppu-Shimabara Graben region (Figure 9.10), whereas the best-fitting GPS block modelling results indicate up

to 8 mm/a of combined strike-slip and extension (Figure 9.5). Slip rates on normal faults in the Kagoshima Graben are no greater than 1 mm/a in the AFRC database (Figure 9.10), whereas the GPS block modelling results suggests that this graben is the site of up to 7 mm/a of extension (Figure 9.5). Although the zone of large left-lateral shear strain cross-cutting southeast Kyushu is associated with numerous left-lateral strike-slip earthquakes (Figure 9.4), there are no mapped active faults (Figure 9.10) which could be accommodating this strike-slip (~7-14 mm/yr; Figure 9.5). These discrepancies suggest that either there may be some gaps in the geological data (i.e., that some faults accommodating active deformation may be un-discovered or hidden, or that some known faults are not sufficiently characterised), or that extensional strain in the Kagoshima Graben and BSG is partly accommodated by dike intrusion and other volcanic/magmatic processes. In some cases, these discrepancies may also be reconciled by testing alternate block model configurations for interpreting the GPS data (although we suspect this will not be able to reconcile most of the discrepancies we observe).

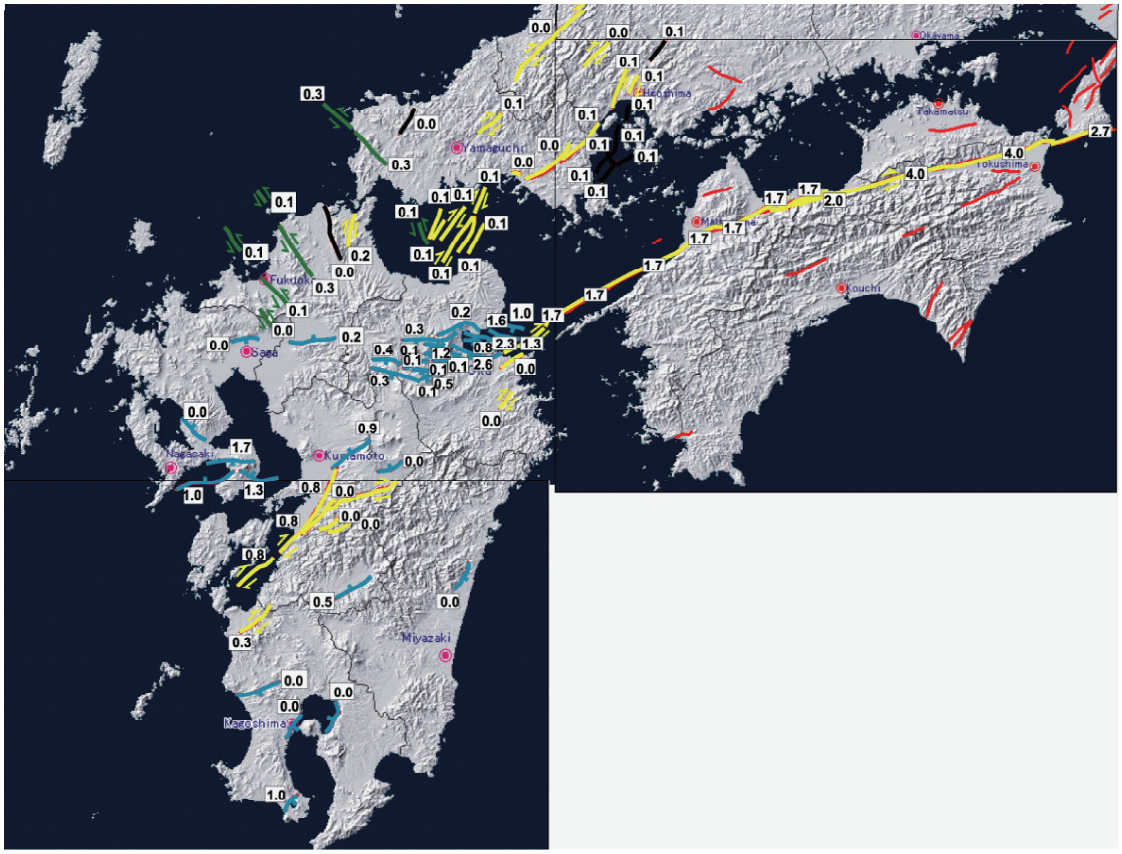

Figure 9.10: Active faults in southwest Japan from the Active Fault Research Centre's active fault database (http://www.aist.go.jp/RIODB/activefault/cgi-bin/index.cgi). The faults are colour-coded by sense of movement (green = dextral, blue = normal, black = reverse, yellow = sinistral. The numbers beside the faults indicate slip rate (mm/a).

9.6.1 Is left-lateral shear in southern Kyushu caused by collision with the Kyushu-Palau Ridge?

Subduction of buoyant features (such as aseismic ridges, oceanic plateaus, and continental fragments) that exist on otherwise normal oceanic plates exert a profound influence on the tectonic and morphological development of subduction margins worldwide (Vogt et al., 1976; McCabe, 1984; Cloos, 1993; Wallace et al., 2005). In some cases, subduction/collision of buoyant features cause curvature (Vogt et al., 1976) and rotation of the subduction margin (McCabe, 1984; Wallace et al., 2005), and deformation of the upper plate (e.g., Marshall et al., 2000; Taylor et al., 1995); in extreme cases, buoyant indentor collision can shut-down subduction, causing it to re-initiate elsewhere (e.g., Cloos, 1993). Margin transverse left-lateral shear in southern Kyushu is localised above the point where there is a change from

subduction of the relatively buoyant Kyushu-Palau Ridge/Shikoku Basin lithosphere (27-15 Ma; Okino et al., 19999) at the Nankai Trough to subduction of more negatively buoyant Cretaceous oceanic lithosphere (Deschamps and Lallemand, 2002) at the Ryukyu Trough (Figure 9.11). We suggest that where buoyant lithosphere is being subducted, the forearc is pushed landward (e.g., northwest) due to the collisional resistance forces transmitted across the plate boundary; conversely, the Cretaceous oceanic slab subducting beneath southwest Kyushu may be rolling back (e.g., Yamaji, 2003), pulling the southern part of the Kyushu forearc seaward relative to the northern half of the forearc. We suggest that these competing effects drive rapid left-lateral shear across southern Kyushu as revealed by GPS and seismicity (Wallace et al., 2009). Similar conceptual models have been proposed to explain deformation of the Costa Rican and New Hebrides forearcs (Marshall et al., 2000; Taylor et al., 1995).

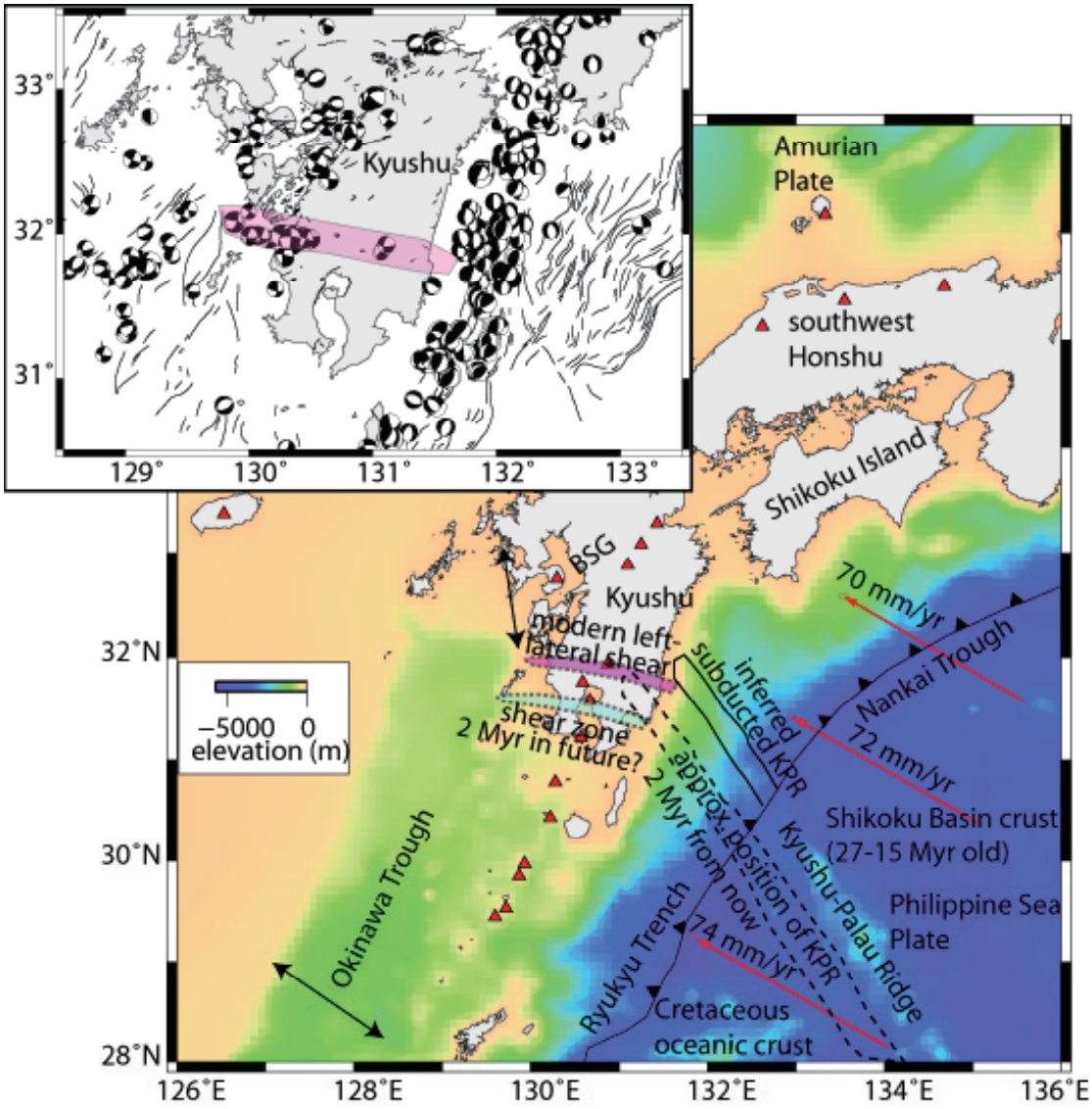

Figure 9.11: Tectonic setting of southwest Japan and schematic illustrating migration of Kyushu/Palau Ridge (KPR) collision point along the Nankai Trough and Ryukyu Trench.

Although GPS and seismological data together argue in favour of active left-lateral strike-slip deformation of southern Kyushu, this interpretation is at odds with the lack of surface faulting evidence for such a shear zone. However, when we consider the Amurian/Philippine Sea Plate relative motion (~70 mm/a pure convergence, with a slight right-lateral sense of ~5 mm/a) and the orientation of the Kyushu-Palau ridge relative to the subduction margin (entering the margin at a 64° angle), we estimate that the Kyushu-Palau ridge subduction

point migrates southwest along the Nankai/Ryukyu trough at ~40 mm/a (or 40 km/Ma) (Figure 9.11). This implies that if the shear zone cross-cutting Kyushu indeed arises from the change in lower plate buoyancy (as we propose here), that the location of this shear zone will follow the Kyushu-Palau ridge subduction point southwest along the margin. Such a continual along-strike migration of the left-lateral shear zone would preclude the accumulation of sufficient surface displacements required to make this a recognizable, through-going fault system at the ground surface.

To test this idea, we have constructed a three-dimensional numerical model of a deforming upper plate (Figure 9.12). The model setup is kept deliberately simple, in order to minimize the number of controlling parameters. Gravity is neglected, the strength of the upper plate is represented by a simple elasto-plastic rheology, and the geometry and strength of a weak visco-elastic region representing the back-arc is imposed (Figure 9.12a).

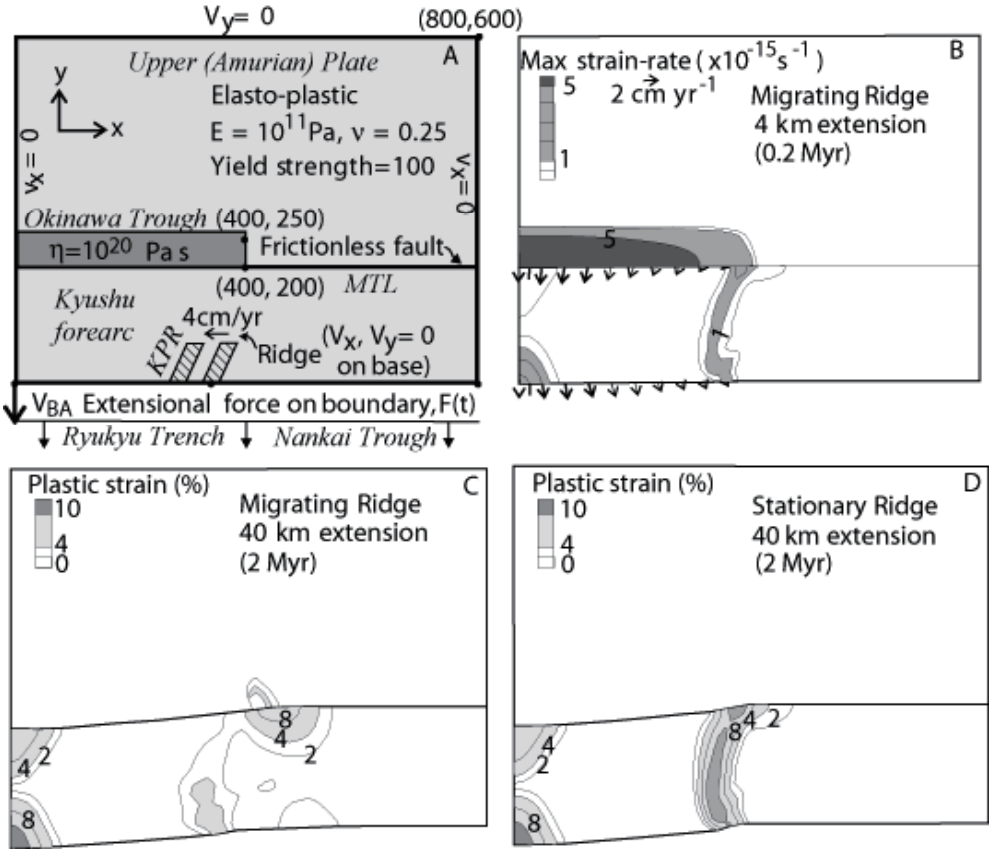

Figure 9.12. (a) Simple three-dimensional model illustrating the effect of a moving ridge on back-arc extension. The model uses the Abaqus/standard finite element code. Model domain is 30 km thick, 800 km long and 600 km wide. The side at y = 0 represents the trench, and an extensional force is applied there with magnitude, *F,* that is adjusted with time to maintain a steady back-arc extension $V_{BA}$of 2 cm/a at the left-hand corner (x = 0, y = 0). The base of the model has zero vertical velocity (out of the page), while horizontal velocity boundary conditions are applied at the other 3 edges of the model as indicated, to prevent material leaving the domain. Rheology is elasto-plastic (light shaded region) and visco-elastic (heavy shaded region, representing a weak back-arc region), where elastic properties of the visco-elastic region are the same as for the rest of the model. A frictionless vertical fault is specified at y = 200 km. Zero horizontal velocities are imposed over a small, basal Section 25 km wide and 60 km long, to simulate the retarding effects of a buoyant ridge on back-arc extension. Tectonic features in southwest Japan corresponding to the numerical model components are labeled in italics. MTL = Median Tectonic Line; KPR = Kyushu-Palau Ridge. (b) Contours of strain rate and velocity vectors early in model evolution (0.2 Ma). Only the left-hand side of the model extends, owing to the presence of a weak viscoelastic region there. (c) Contours of plastic strain after 40 km of extension (2 Ma) for model including ridge migration, illustrating diffuse plastic deformation between the material overlying the ridge, and the corner of the viscoelastic region. (d) Contours of plastic strain after 40 km extension (2 Ma), similar to (c), except that the ridge does not migrate along-strike, producing more focused shear deformation of the forearc.

The subduction interface is simplified to a vertical block boundary at which a spatially uniform extensional force is applied to mimic the effects of rollback, triggering extension in the back-arc region. The magnitude of the force is adjusted automatically during the model run, to reproduce a maximum extensional velocity of 2 cm/a at the left-hand edge, similar to the present rate of extension across the southern back-arc region in Kyushu. The model does not attempt to reproduce compressional effects such as those seen across the Shikoku block in Japan. Model dynamics are therefore simplified and may only be used qualitatively to compare to the tectonics of southwest Japan.

In the model, the effect of a buoyant ridge subduction is simplified to a basal boundary condition, by imposing a region where horizontal velocities are zero (Figure 9.12a). The combined effect of the ridge and the termination along-strike in the visco-elastic region, focus the extensional deformation to the left-hand side, and create a localised, left-lateral shear-zone joining the upper plate immediately above the ridge to the right-hand tip of the visco-elastic back-arc region (Figure 9.12b).

Our ideas regarding the origin of the left-lateral shear zone cutting across southern Kyushu are compatible with results from the simple numerical model, where the ridge is prescribed to move along-strike a rate of 4 cm/a, similar to the along-strike rate of migration of the Kyushu/Palau Ridge. In models where the ridge migrates, plastic strain in the upper plate near to the position of the ridge (Figure 9.12c) remains low and diffuse after 2 Ma of deformation. Conversely, when the ridge is stationary (Figure 9.12d), a zone of localised plastic shear develops above it and cross-cuts the forearc region, with a similar geometry to the contemporary strain-rate pattern (Figure 9.12b). Such a tectonic model will be important to consider in terms of the future rock deformation hazard in Kyushu, because the zone of high shear strain (currently located just north of the Kagoshima Graben) may actually migrate further south (following the Kyushu-Palau Ridge) during the time period of interest.

However, although our explanation of this shear zone as a response to migrating ridge subduction is one viable model for the future tectonic evolution of Kyushu, we must consider other alternative models for the presence of this left-lateral shear zone. For example, it is possible that deformation across this shear zone is currently occurring at a more rapid rate than normal, and that the current rate of strain does not represent the longer-term strain rate across the shear zone. Using the probabilistic methodology we have developed, we can incorporate such alternative models into a tectonic hazard assessment via a logic tree approach. Consultation with Japanese experts on Kyushu tectonics will also facilitate the development of alternate conceptual tectonic models for Kyushu.

9.7 Probabilistic GPS Strain Estimates

9.7.1 Weighted average of GPS strain models from logic tree

To estimate the rock deformation hazard probabilistically using GPS data, we must consider a variety of alternative tectonic models (i.e., using different block and/or fault configurations) to estimate the subduction-related elastic strains, as well as applying a range of smoothing parameters to the strain-rate mapping done with the Haines and Holt method, or use a different strain-rate mapping methodology altogether. An approach that incorporates all viable tectonic models and expert opinions similar to that used in PSHA methodologies is the best way to incorporate all available knowledge about the potential tectonic hazard into a probabilistic rock deformation hazard assessment using GPS. To assess a range of possible strain models from the available GPS data, we construct a logic tree (Figure 9.13) that incorporates the various block model configurations explored in the preceding Sections, as well as implementing different approaches for the strain mapping exercise itself. In terms of the strain mapping approaches, we use the Haines and Holt approach (using a variety of strain variance parameters, see previous discussion), as well as a very simple approach outlined in Miura et al. (2004), where we fit a surface to the GPS velocities, and take spatial derivatives of the surface to estimate strain rates. Our logic tree consists of 120 different branches; we have calculated GPS strain models for each of these branches. We have also weighted each branch of the logic tree (Figure 9.13) based on our own opinion about which models are more or less viable. Ideally, the logic tree would be constructed and weighted via

consultation of an expert panel, similar to what was done for the Tohoku Case Study (Chapman et al., 2009). However, given the limited time frame for the Kyushu Case Study, the expert elicitation exercise was not possible.

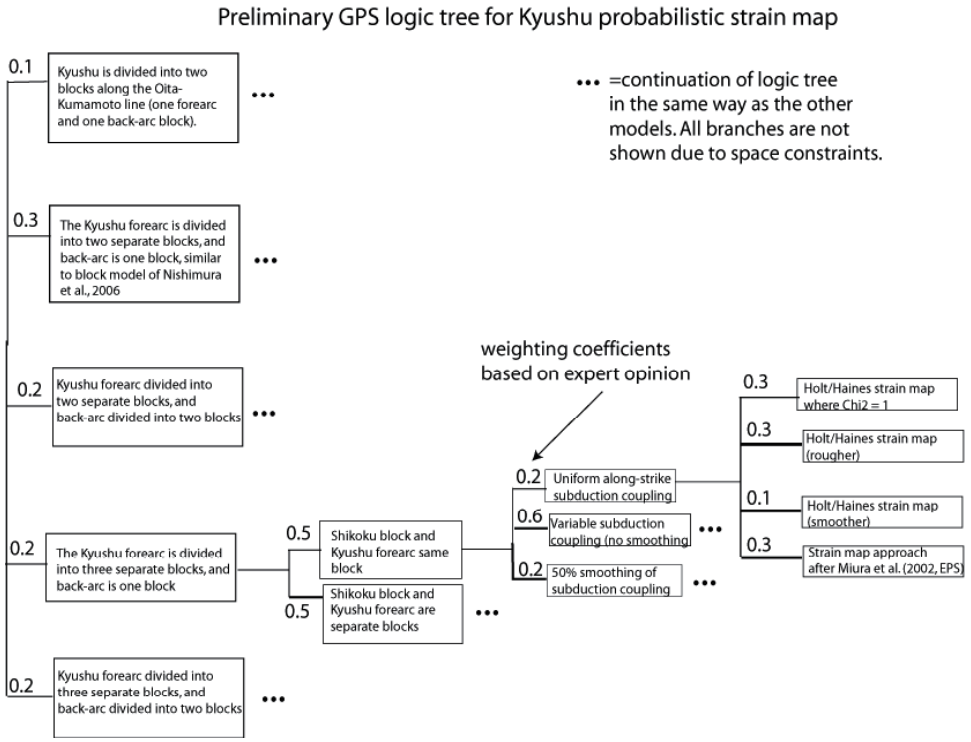

Figure 9.13: Logic tree developed for GPS strain map. Numbers on logic tree branches represent weighting for that logic tree branch.

Figure 9.14 shows a weighted average of all the strain models developed from the logic tree. Given that there is a mix of large shear (Figure 9.14b) and areal strains (Figure 9.14a) within the Kyushu region, we have also chosen to show the strain in terms of the second invariant of the strain tensor (Figure 9.15), which gives us a single measure that incorporates both shear and areal strain. This is largely important to use where we want to use a single strain rate value (rather than both the areal and shear strain values) to determine whether or not there is high or low strain at a given site. The formula for the second invariant of the strain rate tensor (in two dimensions) is: sqrt (Exx^2 + Eyy^2 + 2*Exy^2), where Exx, Eyy, and Exy are the components of the horizontal strain tensor. For reference, the formula for areal strain rate is: Exx +Eyy, and maximum shear strain rate is: sqrt (0.25*(Exx-Eyy)^2 + Exy^2).

Most of the strain patterns obvious in Figures 9.8 and 9.9 are still apparent in the weighted average strain maps (Figure 9.14). For example, the high shear strain cutting across southern Kyushu and along the SE boundary of the Beppu-Shimabara graben are still prominent in the weighted average strain map, suggesting that these features are indeed robust. Similarly high extensional strain persists in the Kagoshima region and southern portion of Kyushu, suggesting that this extensional strain is also real, and not just a model dependent feature.

9.7.2 Histograms of GPS strain values at selected locations in Kyushu

To get an idea of the range of strain rates produced by the different GPS strain models in the logic tree, and to assess the epistemic uncertainties in the GPS strain rate estimates, we can look at histograms (Figure 9.17) of strain rates estimated at several sample locations within Kyushu (Figure 9.16). Similar histograms have also been created for the surface deformation and seismologically-derived strain (see relevant Sections of this report). The strain rates shown are the second invariant of the horizontal strain tensor (to encompass areal and shear strain rates, see discussion in preceding Section).

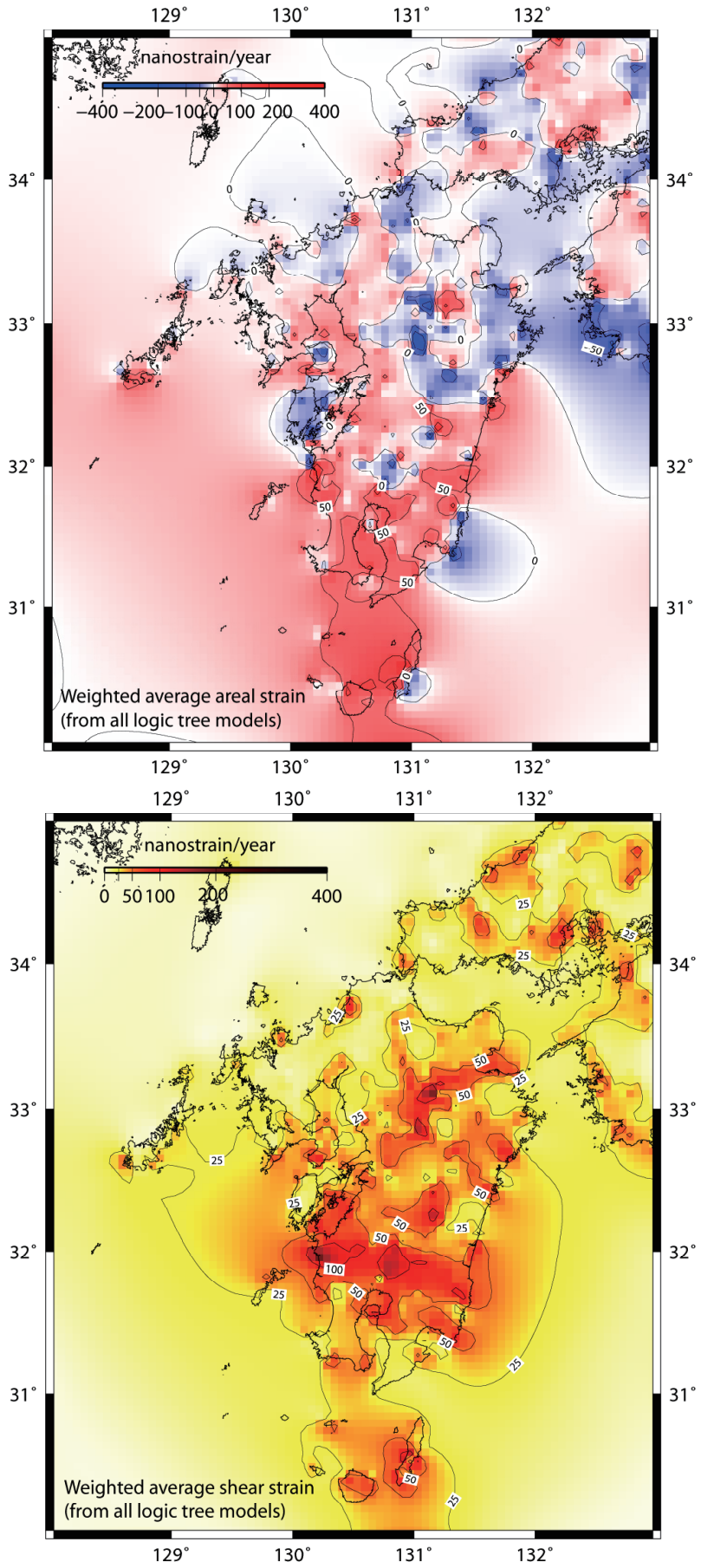

Figure 9.14: Weighted average areal (9.14a) and shear (9.14b) strain (in nanostrains/a) for all 120 strain models from the logic tree (see Figure 9.13).

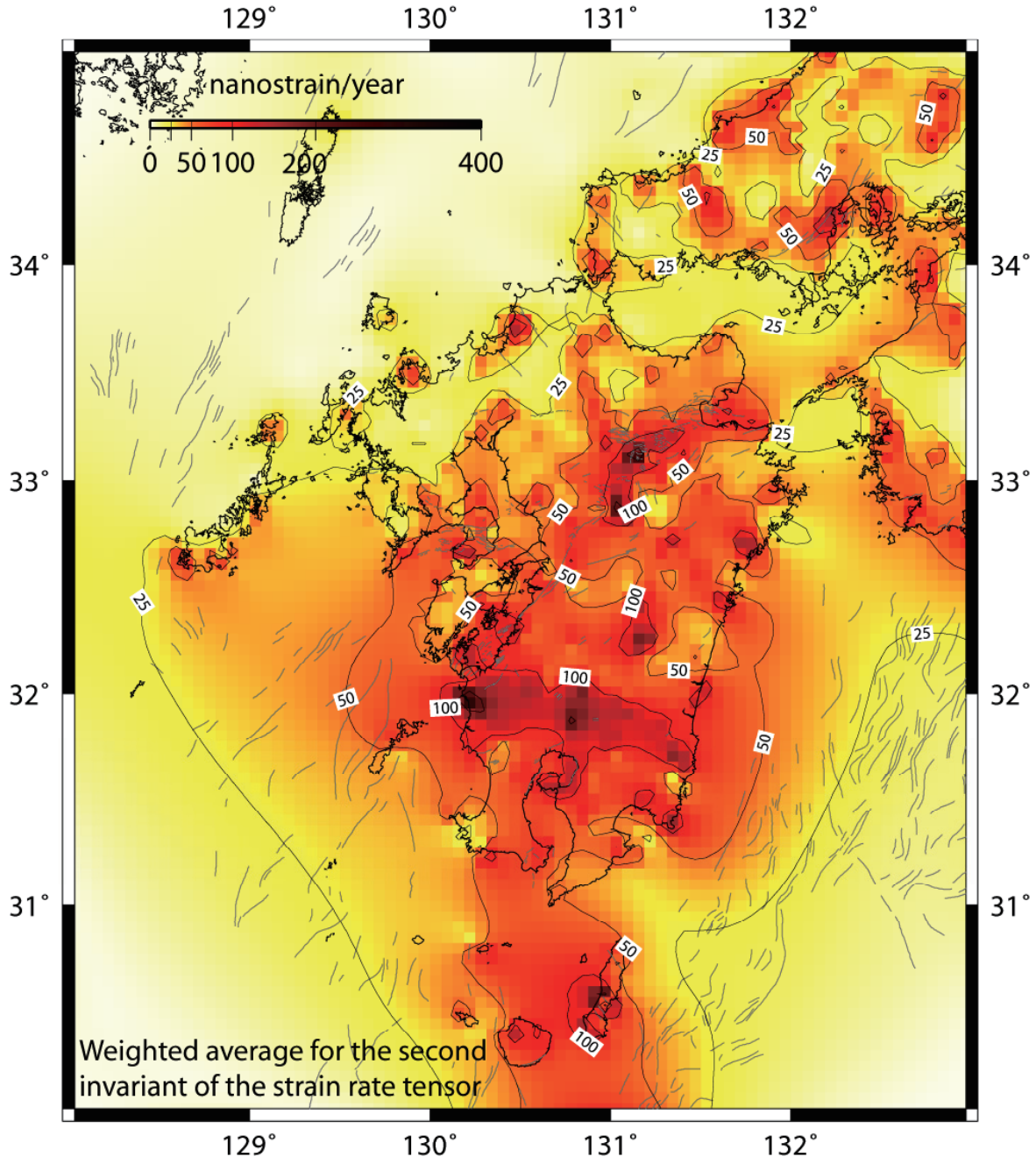

Figure 9.15: Weighted average of the second invariant of the horizontal strain tensor (in nanostrains/a) for all 120 strain models from the logic tree (see Figure 9.13).

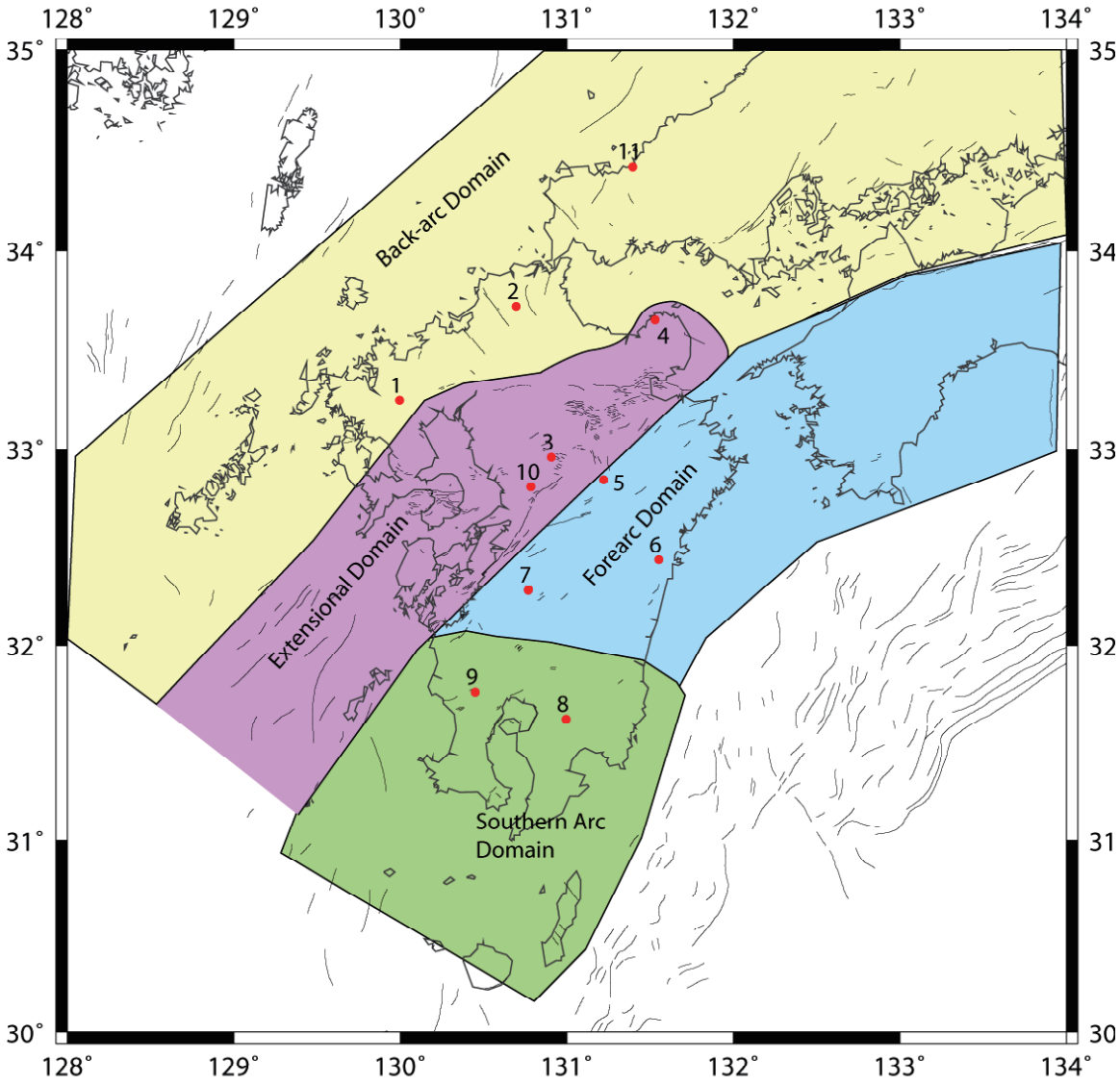

Figure 9.16: Map showing location of sites where we show histograms of GPS-derived strain rates in Figure 9.17. The locations are super-imposed on a map of tectonic domains, discussed in Section 6.

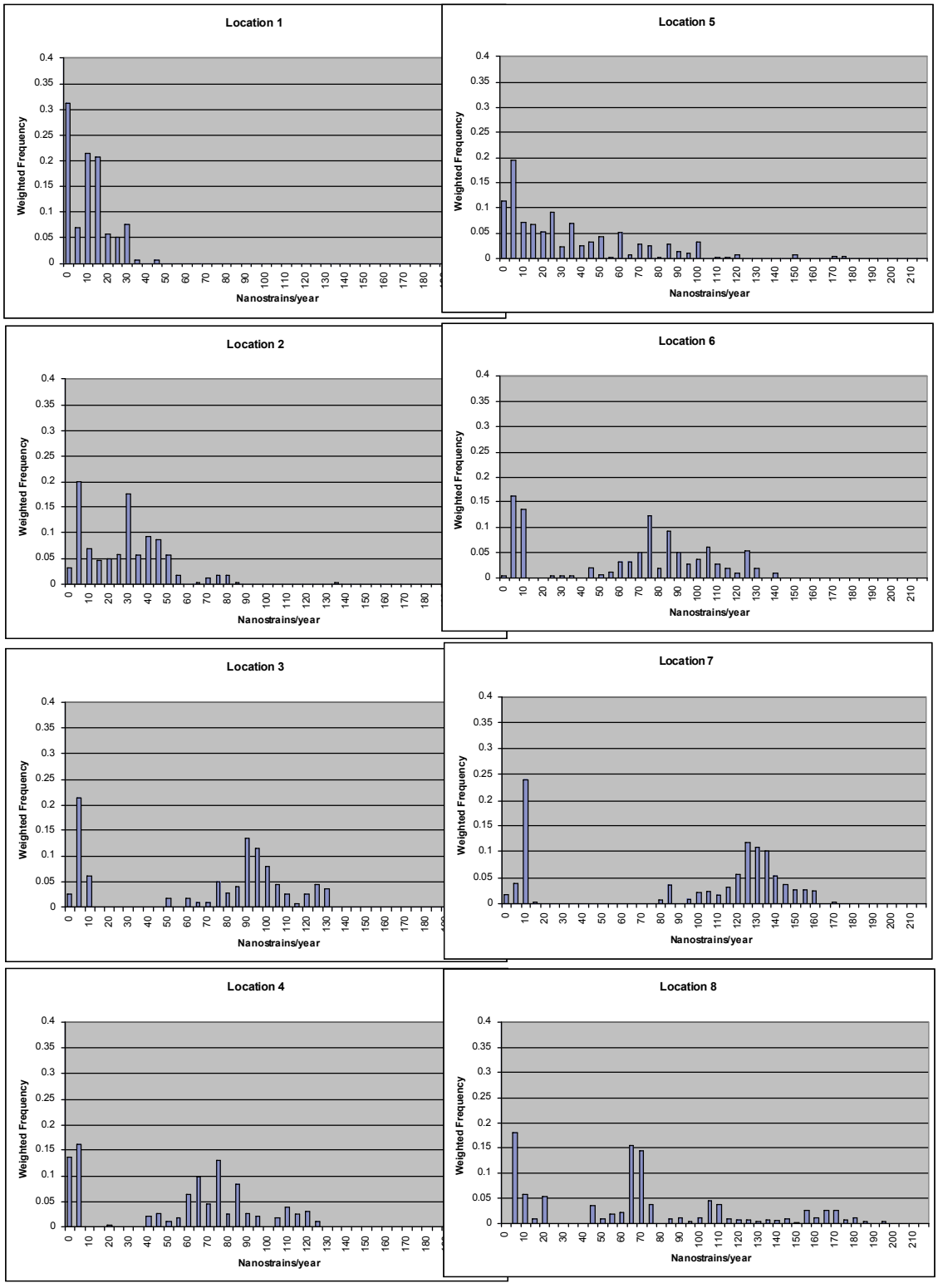

Figure 9.17 (continued on next page): Histogram of GPS strain rates (in terms of weighted frequency) at example locations (see Figure 9.15), after full sampling of the GPS logic tree in Figure 9.13.

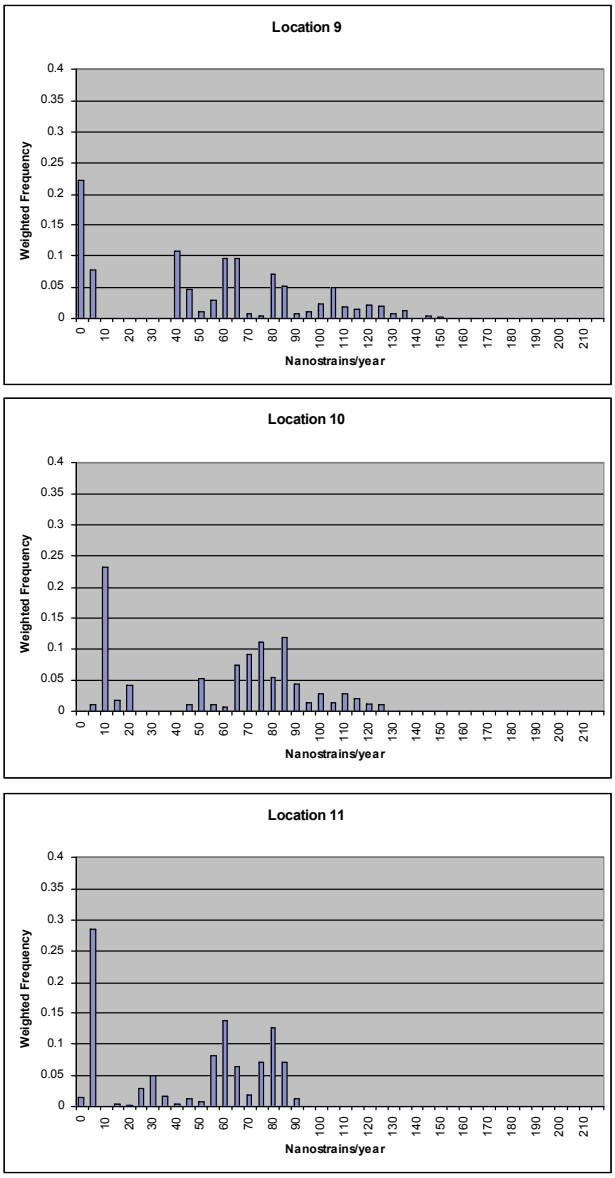

Figure 9.17 (continued from previous page): Histogram of GPS strain rates (in terms of weighted frequency) at example locations (see Figure 9.15), after full sampling of the GPS logic tree in Figure 9.13.

Backarc domain. The histogram for Location 1 shows a relatively narrow distribution of low strain rates from the 120 different strain models, generally less than 20 nanostrains/year. Such low strain rates are consistent with this site being located in the back-arc region, where active fault slip rates are low. Similarly, Location 2 (also in the back-arc region) has strain rates that are generally low (< 40 nanostrains/year), but with a slightly wider distribution of strain rates than Location 1 (indicating slightly higher uncertainties in the strain rates at Location 2 compared to Location 1). Location 11 has higher strain rates than the other back-arc sites, which we think are likely due to effects on the GPS site velocities from the nearby west Tottori earthquake in 2000 (magnitude 7.3), and may not reflect actual background tectonic strain rates.

Extensional Arc domain. Location 3, has a relatively narrow distribution of high strain rates (averaging ~100 nanostrains/year), consistent with its position within a zone of active tectonic extension. The lowest strain rate values in this histogram come from the strain estimates

using the Miura et al. (2004) approach to calculating strain. We suspect that this approach excessively smooths the strain values, hence the very low strain rates we obtain here. In the future, we would recommend strongly down-weighting the strain results using this approach, as these results are probably overly smoothed. The lowest strain rates in the other histograms shown here also contain this problem. Although Location 4 is also in the Extensional Arc domain, and also has reasonably high strain rates, probably due to the close proximity to active faults of the BSG. Location 10 is also within the BSG, and as expected shows a concentration of high strain rates from the GPS strain models, generally around 70-90 nanostrains/year.

Forearc domain. Example locations in this domain exhibit a broad range of strain rates. Location 5, which is close to the southern edge of the BSG shows a broad range of strain rates, but most of them are quite low, < 40 nanostrains/year. These low strain estimates are somewhat surprising given the close proximity of this site to active faulting in the BSG. Location 6 has a surprisingly high strain rate for the forearc domain, ~70-110 nanostrains/year, although it is located close to the continuation of an active fault trend (see Section discussing discrimination of tectonic domains and selection of example locations) and on the edge of an area of moderately high uplift rate (see the strain rates from surface deformation Section). The high strain rates at Location 6 may also be related to imperfect subduction coupling models; perhaps we have not completely removed the elastic strain effect related to interseismic subduction interface coupling, and that has influenced the strain rates there. Location 7 has some of the highest strain rates of any of the locations, generally 120-140 nanostrains/year. This is surprising, given the long distance of this example location from the known, active faults. However, this location is probably also in a region of high shear strain related to the left-lateral shear zone that we have identified cutting across southern Kyushu, as well as any extension along the southeastern margin of the BSG.

Southern Arc domain. Locations 8 and 9 show a large spread of strain rate estimates, indicating a higher uncertainty in the strain rates in those locations. However, most of the strain rates are >50 nanostrains/year, and are up to 140-180 nanostrains/year, so this region does appear to be a generally high strain area. Location number 8 is located on a low slip rate active fault (see Section 8). Strain at both of these example locations is probably influenced by extension in the Kagoshima Graben region, as well as the strong left-lateral shear strain zone cutting across southern Kyushu.

9.8 Notes and Caveats

One of the advantages of the probabilistic approach is that it allows us to assess some of the uncertainties inherent in the strain rate estimates (e.g., epistemic uncertainties due to choice of tectonic models and/or modelling techniques). However, we must also ensure that we have accurately estimated the uncertainties in the GPS velocity data. The large sample interval (3 months) of the GPS timeseries data available to us for this study means that reliable noise models for the GPS data could not be developed. This affects the estimation of uncertainty in the point GPS velocities, which translates into additional uncertainty in the strain-rate estimates. A more complete temporal sampling of the CGPS dataset, and rigorous estimation of changes in CGPS site position due to earthquakes, equipment changes, etc. would improve the velocity estimates substantially, and lower the resulting uncertainties. Additionally, the GPS station spacing is still quite large compared to the 5-km grid over which strain rates are required. In some parts of Japan there are more GPS stations (campaign and continuous, operated by various Japanese universities and other organisations) in addition to the GSI-run Geonet network, and data from these could contribute greatly to an improved strain-rate estimation. Moreover, as longer GPS datasets are collected, the GPS velocity uncertainties will slowly decrease. Also, the velocity uncertainties will become more reliable when proper noise models are adopted. Both these improvements (as well as GPS velocity data from additional sites) would allow us to refine the results of the GPS strain-rate study described here.

9.9 References for Section 9

Altamimi, Z., P. Sillard, and C. Boucher (2002), ITRF2000: A new release of the International Terrestrial Reference Frame for earth science applications, J. Geophys. Res., 107(B10), 2214, doi:10.1029/2001JB000561.

Aramaki, S., 1984, Formation of the Aira Caldera, southern Kyushu, 22,000 years ago, J. Geophys. Res., 89(B10), 8485-8501.

Beavan, J., and, J. Haines (2001), Contemporary horizontal velocity and strain-rate fields of the Pacific-Australian plate boundary zone through New Zealand, *J. Geophys. Res. 106*, 741-770.

Beavan, J., P. Tregoning, M. Bevis, T. Kato, and C. Meertens (2002), The motion and rigidity of the Pacific Plate and implications for plate boundary deformation, *J. Geophys. Res.*, *107,* 2261, doi:10.1029/2001JB000282.

Beutler, G., H. Bock, E. Brockmann, R. Dach, P. Fridez, W. Gurtner, U. Hugentobler, D. Ineichen, J. Johnson, M. Meindl, L. Mervart, M. Rothacher, S. Schaer, T. Springer, R. Weber (2001), Bernese GPS Software Version 4.2, Ed. by U. Hugentobler, S. Schaer, P. Fridez, *Astronomical Institute, University of Berne.*

Bird, P., 2003, An updated digital model of plate boundaries, Geochem. Geophys. Geosyst., 4(3), 1027, doi:10.1029/2001GC000252.

Calais E., M. Vergnolle, V. San'kov, A. Lukhnev, A. Miroshnitchenko, S. Amarjargal, J. Déverchère, 2003, GPS measurements of crustal deformation in the Baikal-Mongolia area (1994–2002): Implications for current kinematics of Asia, *J. Geophys. Res., 108 (B10)*, 2501, doi:10.1029/2002JB002373.

Chapman, N., M. Apted, J. Beavan, K. Berryman, M. Cloos, C. Connor, L. Connor, O. Jaquet, N. Litchfield, S. Mahony, W. Smith, S. Sparks, M. Stirling, P. Villamor and L. Wallace (2009). Development of Methodologies for the Identification of Volcanic and Tectonic Hazards to Potential HLW Repository Sites in Japan: The Tohoku Case Study. Nuclear Waste Management Organisation of Japan, Tokyo. Technical Report: NUMO-TR-08-03. 135 pps.

Cloos, M., 1993, Lithospheric buoyancy and collisional orogenesis; subduction of oceanic plateaus, continental margins, island arcs, spreading ridges, and seamounts, GSA Bulletin, 105: 715-737.

Deschamps, A., and S. Lallemand, The West Philippine Basin: An Eocene to early Oligocene back arc basin opened between two opposed subduction zones, *J. Geophys. Res.*, *107*(B12), 2322, doi:10.1029/2001JB001706, 2002.

Fujiwara, S., H. Yarai, S. Ozawa, M. Tobita, M. Murakami, H. Nakagawa, and K. Nitta, 1998, Surface displacement of the March 26, 1997, Kagoshima-ken-hokuseibu earthquake in Japan from synthetic aperture radar interferometry, *Geophys. Res. Lett., 25(24)*, 4541-4544.

Gutscher, M.-A., and S. Lallemand, 1999, Birth of a major strike-slip fault in SW Japan, Terra Nova, 11(5), 203-209.

Haines, A. J., W. E. Holt, A procedure for obtaining the complete horizontal motions within zone of distributed deformation from the inversion of strain rate data, J. Geophys. Res., 98(B7), 12057-12082, 10.1029/93JB00892, 1993.

Heki, K., S. Miyazaki, H. Takahashi, M. Kasahara, F. Kimata, S. Miura, N. Vasilenco, A. Ivashchenco and K. An, The Amurian plate motion and current plate kinematics in Eastern Asia, J. Geophys. Res., 104, 29147-29155, 1999.

Herring, T. A., 2001, GLOBK global Kalman filter VLBI and GPSanalysis program, version 5.03, Mass. Inst. of Technol., Cambridge.

Hirose, H., K. Hirahara, F. Kimata, N. Fujii, and S. Miyazaki, 1999, A slow thrust slip event following the two 1996 Hyuganada earthquakes beneath the Bungo Channel, southwest Japan, *Geophys. Res. Lett., 26(21)*, 3237-3240.

Ito, T., T. Ikawa, S. Yamakita, and T. Maeda, Gently north-dipping Median Tectonic Line (MTL) revealed by recent seismic reflection studies, southwest Japan, *Tectonophys.*, 264, 51–63, 1996

Kodama, K., H. Tashiro, and T. Takeuchi (1995), Quaternary counterclockwise rotation of south Kyushu, southwest Japan, *Geology, 23,* 823-826, 1995.

Kriswati, E. and Iguchi, M., 2003, Inflation of the Aira Caldera prior to the 1999 eruptive activity at Sakurajima Volcano detected by GPS network in south Kyushu, Disaster Prevention Research Institute Report, 46, 817-825.

Langbein J. (2004), Noise in two-color electronic distance meter measurements revisited, *J. Geophys. Res., 109*, B04406, doi:10.1029/2003JB002819.

Marshall, J. S., D. M. Fisher, T. W. Gardner, Central Costa Rica deformed belt: Kinematics of diffuse faulting across the western Panama block, Tectonics, 19(3), 468-492, 10.1029/1999TC001136, 2000.

McCabe, R., 1984, Implications of palemagnetic data on the collision-related bending of island arcs: Tectonics, 4, 409-428.

McCaffrey, R. (1995), DEF-NODE users guide, Rensselaer Polytechnic Inst., Troy, N.Y.

McCaffrey, R., M.D. Long, C. Goldfinger, P.C. Zwick, J.L. Nabelek, C.K. Johnson, and C. Smith (2000), Rotation and plate locking at the southern Cascadia subduction zone, *Geophysical Research Letters, 27*, 3117-3120.

McCaffrey, R. (2002), Crustal block rotations and plate coupling: *in* Stein, S., and Freymueller, J., eds., Plate Boundary Zones, AGU Geodynamics Series v. 30, p. 100-122.

McCaffrey, R., 2005. Block kinematics of the Pacific-North America plate boundary in the southwestern United States from inversion of GPS, seismological and geologic data, *J. geophys. Res.,* **110**, doi:10.1029/2004JB003307.

McClusky, S. et al., 2001. Present day kinematics of the eastern California Shear zone from a geodetically constrained block model, *Geophys. Res. Lett.,* **28**, 3369-3372.

Meade, B.J., and Hager, B.H., 2005. Block models of crustal motion in southern California constrained by GPS measurements, *J. geophys. Res.,* **110**, B03403, doi:10.1029/2004JB003209.

Miura, S., T. Sato, A. Hasegawa, Y. Suwa, K. Tachibana and S. Yui, 2004, Strain concentration zone along the volcanic front derived by GPS observations in the NE Japan arc, *Earth Planets Space, 56*, 1347-1355.

Nishimura, S. Hashimoto, M., and Ando, M., 2004, A rigid block rotation model for the GPS derived velocity field along the Ryukyu arc, Phys. Earth Planet. Inter. 142, 185-203.

Nishimura, S. and M. Hashimoto, 2006, A model with rigid rotations and slip deficits for the GPS-derived velocity field in Southwest Japan, *Tectonophysics, 421*, 187-207.

Okada, A., 1970, Fault topography and rate of faulting along the Median Tectonic Line in the drainage basin of the River Yoshino, northeastern Shikoku, Japan (in Japanese with English abstract), Geogr. Rev. Jpn., 43, 1-21.

Okada, A., 1973, Quaternary faulting along the Median Tectonic Line in the central part of Shikoku (in Japanese with English abstract), Geogr. Rev. Jpn., 46, 295-322.

Okino, K., Y. Ohara, S. Kasuga, and Y. Kato (1999), The Philippine Sea: New survey results reveal the structure and the history of the marginal basins, *Geophys. Res. Lett.*, *26*, 2287–2290

Onishi, M., T. Ikawa, T. Matsuoka, T. Kawamura, T. Echigo, M. Orito, T. Ito, N. Hirata, T. Iwasaki, E. Kurashimo, and H. Sato, Deep seismic reflection experiment with a highly

dense array of seismograms near the Median Tectonic Line, Shikoku, Japan, *Abstr. 1999 Fall Meeting of the Seismological Society of Japan*, P107, 1999.

Prawirodirdjo, L. and Y. Bock (2004): Instantaneous global plate motion model from 12 years of continuous GPS observations, J. Geophys. Res., 109, B08405, doi:10.1029/2003JB002944.

Rothacher, M., and L. Mervart (eds.), Documentation of the Bernese GPS Software Version 4.0, 418 pp, Astron. Inst., Univ. of Bern, Bern, Switzerland, 1996.

Sagiya, T. and W. Thatcher (1999), Coseismic slip resolution along a plate boundary megathrust: The Nankai Trough, southwest Japan, J. Geophys. Res., 104(B1), 1111-1129.

Sagiya, T., S. Miyazaki, and T. Tada (2000), Continuous GPS array and present-day crustal deformation of Japan, *Pure and Applied Geophysics,* 2303-2322.

Sella, G.F., T.H. Dixon, and A.L. Mao, 2002, REVEL: A model for recent plate velocities from space geodesy: *J. of Geophys. Res., v. 107(B4),* doi:10.1029/2000JB000033.

Shiomi, K., H. Sato, K. Obara, and M. Ohtake, 2004, Configuration of the subducting Philippine Sea plate beneath southwest Japan revealed from receiver function analysis based on multivariate autoregressive model, *J. Geophys. Res., 109(B040308)*, doi:10.1029/2003JB002774.

Tabei, T., and eleven co-authors, 2002, Subsurface structure and faulting of the Median Tectonic Line, southwest Japan inferred from GPS velocity field, *Earth Planets Space, 54*, 1065-1070.

Taylor, F.W., and ten co-authors, 1995, Geodetic measurements of convergence at the New Hebrides island arc indicate arc fragmentation caused by an impinging aseismic ridge, *Geology*, 23(11), 1011-1014.

Vogt, P.R., Lowrie, A., Bracey, D.R., and Hey, R.N., 1976, Subduction of aseismic oceanic ridges: Effects on shape, seismicity, and other characteristics of consuming plate boundaries: Geological Society of America Special Paper 172, 59 p.

Wallace, L.M., J. Beavan, R. McCaffrey and D. Darby, 2004, Subduction zone coupling and tectonic block rotations in the North Island, New Zealand, *J. Geophys. Res.*, 109(B12), doi: 10.1029/2004JB003241.

Wallace, L.M., McCaffrey, R., Beavan, J., and Ellis, S., 2005, Rapid microplate rotations and backarc rifting at the transition between collision and subduction, *Geology, 33***:** 857-860.

Wallace, L.M., J. Beavan, R. McCaffrey, K. Berryman, and P. Denys, 2007, Balancing the plate motion budget in the South Island, New Zealand using GPS, geological and seismological data, *Geophys. J. Int.,* doi: 10.1111/j.1365-246X.2006.03183.x

Wallace, L.M., S. Ellis, K. Miyao, S. Miura, J. Beavan, and J. Goto, 2009, Enigmatic, highly active left-lateral shear zone in southwest Japan explained by aseismic ridge collision, *Geology, 37(2)*, 143-146.

Williams S. D. P., Y. Bock, P. Fang, P. Jamason, R. M. Nikolaidis, L. Prawirodirdjo, M. Miller, D. J. Johnson (2004), Error analysis of continuous GPS position time series, *J. Geophys. Res., 109,* B03412, doi:10.1029/2003JB002741.

Yagi, Y., M. Kikuchi, and T. Sagiya, 2001, co-seismic slip, post-seismic slip, and aftershocks associated with two large earthquakes in 1996 in Hyuga-nada, Japan, *Earth Planets Space, 53,* 793-803.

Zhang, J., Y. Bock, H. Johnson, P. Fang, S. Williams, J. Genrich, S. Wdowinski, and J. Behr (1997), Southern California Permanent GPS Geodetic Array: Error analysis of daily position estimates and site velocities, *J. Geophys. Res.*, *102*(B8), 18,035–18,056.